UNIVERSITÀ
DI PAVIA

Dipartimento di Biologia e Biotecnologie “L. Spallanzani”

Laurea Magistrale in Neurobiology

The Central Nervous System in Osteogenesis Imperfecta: *in vivo* evaluation of oxidative stress in the cerebellum of the Brtl murine model

Supervisor:

Prof. Fabrizio De Luca

Co-supervisor:

Prof. Maria Grazia Bottone

Experimental thesis by

Emma Lugli

Academic year 2023/2024

Table of contents

1. Introduction

1.1. The cerebellum

The cerebellum, whose name comes from the Latin *cerebellum*, which means 'small cerebrum', is a subcortical brain structure involved in both motor and nonmotor functions and represents the largest portion of the hindbrain (Jimsheleishvili & Dididze, 2024). Despite representing only 10% of the whole brain volume, both in humans and in mice the cerebellum contains more than half of the total neurons. Different regions of the cerebellum receive projections from several distinct brain areas and spinal structures and then project back to the brain, creating circuits known as *cerebellar loops*; indeed, the cerebellar cortex is composed of regular and repeating units, each containing the same core microcircuit (Lara-Aparicio et al., 2022). It is a distinct and recognisable feature of vertebrates' brains: exception made for the more primitive chordates, all vertebrates have a cerebellum-like structure and share the same developmental pattern. The structure of the cerebellum has been maintained virtually unaltered in mammals and birds whereas in fish, amphibians and reptiles displays some differences. Nonetheless, in all vertebrates maintains the same functional organization: input cells receive sensory stimuli and originate a response through output cells (Sultan & Glickstein, 2007).

1.1.1 Anatomy and gross morphology

Separated from the cerebral *occipital lobe* by the *tentorium cerebelli*, the cerebellum is situated in the posterior cranial fossa and contacts the inferior colliculi of the mesencephalon rostrally and the IV ventricle and brainstem ventrally (**Figure 1**). In parasagittal sections, the cerebellum shows a well-defined macroscopic organization: the outer cerebellar cortex (grey matter) and the inner white matter (*arbor vitae,* so called for its tree-like structure) containing three pairs of deep nuclei (**Figure 2**). The surface of the cerebellum is highly convoluted both in humans and mice. Constituted by two hemispheres, separated by the *falx cerebri*, the morphology of the cerebellum consists of a cortical layer that envelops a substantial core of white matter. The cerebellar cortex is a large sheet of folds with a uniform structure composed of three cell layers. Within the white matter are the cerebellar nuclei which receive inputs primarily from the cerebellar cortex and generate the output to the brainstem and structures of the thalamus (Schröder et al., 2020).

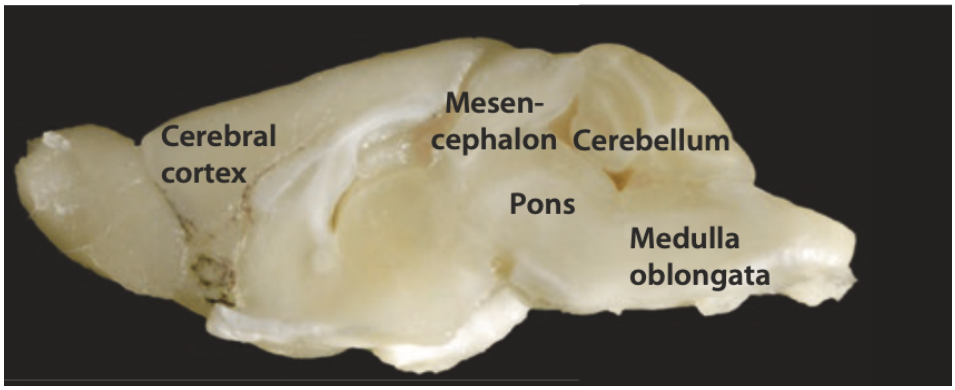

Figure 1 Midsagittal section of a mouse brain: the cerebellum is located in the dorsocaudal portion of the brain, borders the mesencephalic inferior colliculi (rostrally) and the brainstem and forth ventricle (ventrally) (modified from Schröder et al., 2020).

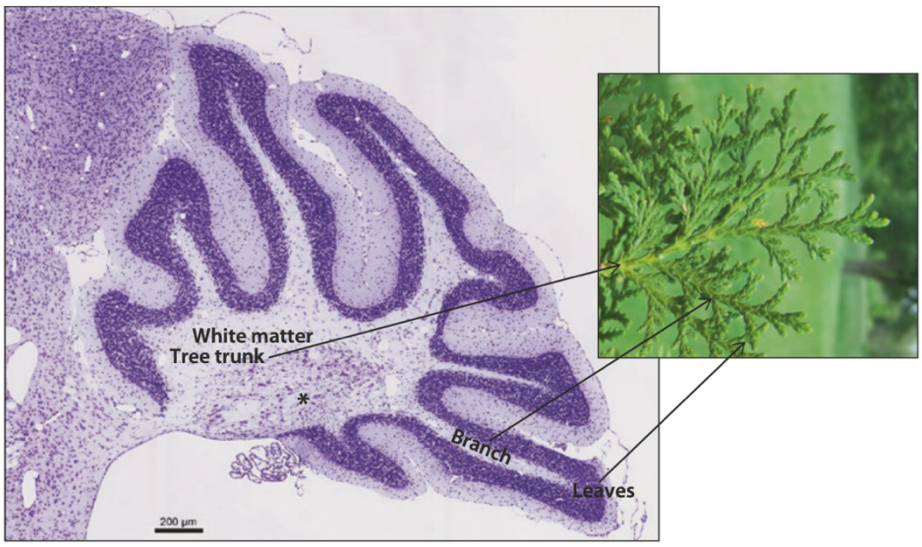

Figure 2. Parasagittal section of a mouse cerebellum: the white matter, bordered by the cerebellar cortex, branches out into a tree-like shape (the arbor vitae) where the 'trunk' contains the deep cerebellar nuclei (modified from Schröder et al., 2020).

The mammalian cerebellum can be divided into three anatomical regions, depending on their progressive development along evolution: (i) the *archicerebellum*, constituting the most primordial division, (ii) the paleocerebellum, the phylogenetically intermediate portion, and (iii) the *neocerebellum*, so called for its relatively recent phylogenetic origin.

From a structural point of view, the cerebellum can be divided into a central *vermis* and two lateral symmetrical hemispheres on the borders (**Figure 3**). The *cerebellar vermis* extends medially to the cerebellar cortex and connects the two cerebellar hemispheres (Butler & Hodos, 2005). The outside of the cerebellum is enveloped by the meninges, which consist of three protective membranous layers surrounding the nervous system. From innermost to outermost

we found: (i) the *pia mater*, highly vascularised and composed of delicate connective tissue, (ii) the *arachnoid*, a thin and impermeable membrane and (iii) the *dura mater*, the tougher meningeal layer (Snell, 2010). In the brain and specifically in the cerebellum, these membranes are integral as protective barriers and functional structures, supporting overall cerebellar health (Snell, 2010).

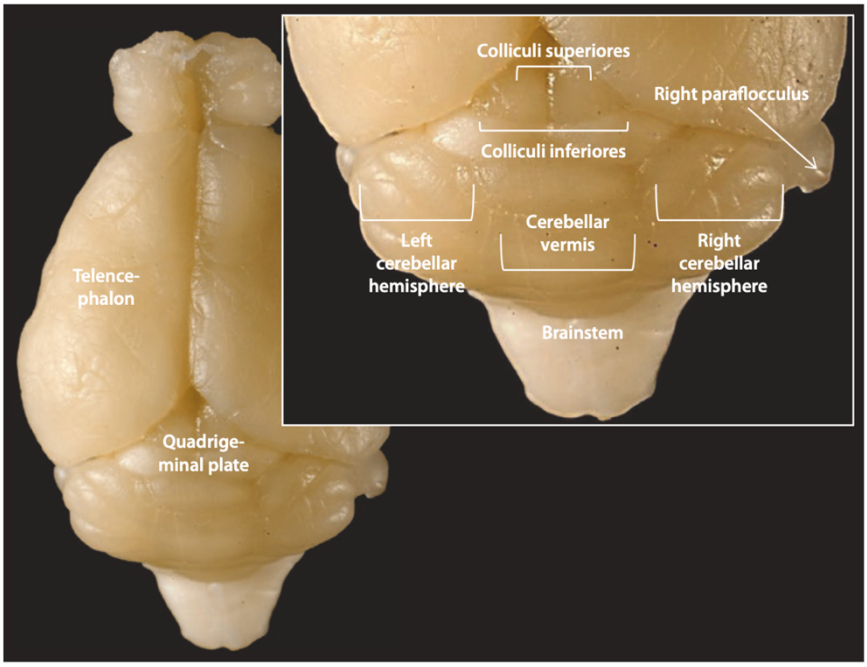

Figure 3. Dorsal view of a mouse brain: in the cerebellum, the transversal grooves neatly separate the vermis from the hemispheres (modified from Schröder et al., 2020).

The *pia mater* adheres to the folds of the cerebellar cortex and supplies the cerebellum with oxygen and nutrients through a dense network of blood vessels. The *tela choroidea* is a two-layer fold of *pia mater* situated between the fornix and the upper thalamus; it fuses with the ependyma forming the *choroid plexus* (CP), an epithelial-like structure that covers a network of fenestrated capillaries. The *choroid plexus* is the major site of production and release of the cerebrospinal fluid (CSF) into the ventricles. In the mouse, the development of the *choroid plexus* begins at E11: at this stage, the first microvilli start forming and they will continue to increase in number as development progresses, becoming longer and slenderer and expanding the surface area of the CP (Schröder et al., 2020). As development progresses, the *choroid plexus* contributes to the maintenance of central nervous system (CNS) homeostasis, forming a neuroprotective barrier for the brain, secreting and controlling the composition of the CSF, and, consequently, influencing the stem cells functions, lining the ventricles and overall regulating

neurogenesis (Johansson, 2014). The *choroid plexus* at the roof of the fourth ventricle secretes the CSF that, flowing through the ventricle, bathes the brainstem and cerebellum (**Figure 4**). In the CNS the CSF plays crucial roles, providing nutrients, removing waste and metabolic products, and protecting from trauma (Schröder et al., 2020).

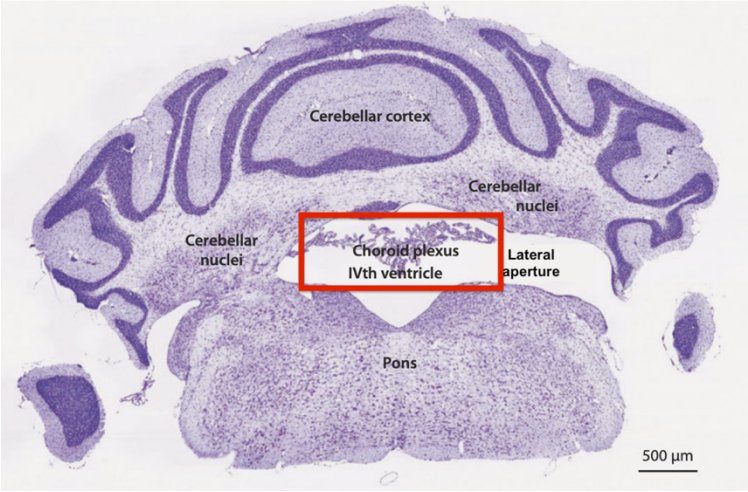

Figure 4. Coronal section of an adult mouse cerebellum; the fourth ventricle *choroid plexus* is framed in red (modified from Schröder et al., 2020).

The *arachnoid mater* is a delicate membrane, impermeable to the CSF, separated from the *pia mater* by the subarachnoid space, which is filled with the CSF entering through three foramina of the fourth ventricle. On the other side we found the subdural space, representing a virtual separation of the *arachnoid* from the *dura mater* (Schröder et al., 2020).

The *dura mater*, conventionally subdivided into the endosteal layer (periosteum lining the inner surface of the skull) and the meningeal layer or proper dura (a denser fibrous membrane), creates folds, specialized extensions creating fundamental structures from brain stability and compartmentalization; in this regard, two folds are particularly relevant to the cerebellum: (i) the *tentorium cerebelli*, a crescent-shaped fold lining the posterior cranial fossa and forming a tent-like shape that covers the cerebellum and separates it from the cerebrum, (ii) and the *falx cerebelli*, a small, sickle-shaped vertical fold sitting between and protecting the two cerebellar hemispheres (Snell, 2010). In addition to their protective and supportive roles, the meninges actively participate during CNS development. Proximal to the developing brain, these specialized membranous layers provide several molecules that regulate neuronal differentiation

and migration (Siegenthaler & Pleasure, 2011); particularly, meningeal cells secrete high levels of collagen type I (Wareham et al., 2024).

In the mouse, the white matter of the cerebellum contains the proper, or deep, cerebellar nuclei: the *emboliform* nucleus, the *dentate* nucleus, and the *interposed* nucleus formed by the *globose* and *fastigial* nuclei. These nuclei are located bilaterally in the white matter of the cerebellum and form the cerebellar output structures. Three groups of fibers constitute the cerebellar white matter: intrinsic fibers (connecting different portions of the cerebellum), afferent fibers (the input of the cerebellum, entering the cerebellum mainly through the inferior and middle cerebellar peduncles) and efferent fibers (the output of the cerebellum) (Schröder et al., 2020). The functional classification of the cerebellum accounts for the *vestibulocerebellum*, *spinocerebellum*, and *cereberocerebellum*. The *vestibulocerebellum*, roughly corresponding to the archicerebellum, includes the *flocculonodar lobe* and *vermis*; it is involved in the regulation of axial musculature (required for the posture control, both at rest and in movement), vestibular reflexes (for balance maintenance) and eye movement. The *spinocerebellum*, comparable to the *paleocerebellum*, corresponds to the *anterior lobe*; involved in postural and gait control, it promotes communication between the cortex and brainstem motor centres. The *cerebrocerebellum*, which corresponds to the *neocerebellum*, occupies the anterior lobe and hemispheres and holds both sensorimotor and non-sensorimotor functions: it engages in the planning, execution and coordination of movements, acting as a 'coordinator' and 'comparator' between motor plans and the final action performance; furthermore, it is involved in cognitive and emotional processing, working memory, language, spatial and executive tasks, e.g. complex decision making tasks (Lara-Aparicio et al., 2022).

1.1.2. The cerebellar cortex

In the cerebellar cortex of adult mice, a series of parallel fissures defines the characteristic pattern of *foliae*, which reminds of the canonical circumvolutions of the cerebral cortex; indeed, the presence of this foliated pattern allows for a larger cortical surface (Chizhikov et al., 2010). The cerebellar cortex can be divided into three main lobes (*anterior, middle* and *flocculonodular lobes*), defined by two transversal fissures. A total of seven fissures defines ten smaller lobules (I-X): lobules I-V are located in the most anterior part of the *vermis*, lobules VI-IX are situated posteriorly and subsequently arises lobule X (which corresponds to the flocculonodular lobe) (**Figure 5**) (Kandel, 2021).

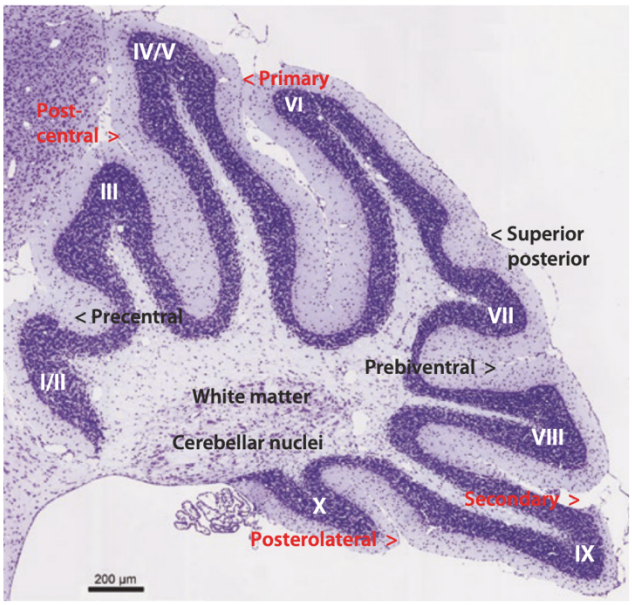

Figure 5. Sagittal section of a mouse cerebellum: the cerebellar cortex of an adult mouse is organized into ten lobules (I-X, in white), separated by seven fissures; the four cardinal fissures are indicated in red (modified from Schröder et al., 2020).

The cells of the cerebellar cortex are organized into three functionally distinct layers, which from the deepest to the most superficial are divided into: (i) the internal granular layer (IGL), (ii) the Purkinje cell layer (PCL), and (iii) the molecular layer (ML) (**Figure 6**) (Schröder et al., 2020).

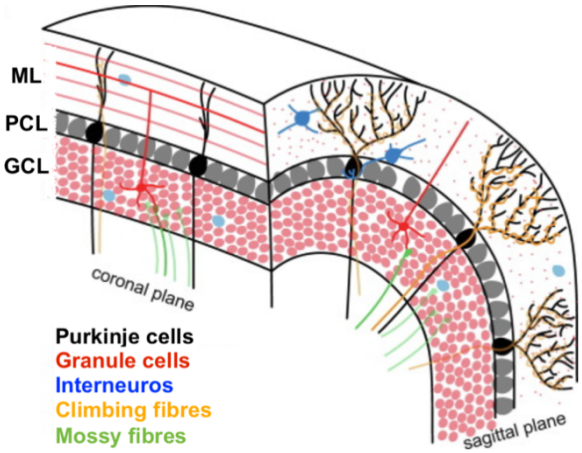

Figure 6. Schematic representation of the cerebellar cortex: organization into three functional layers, molecular layer (ML), Purkinje cell layer (PCL) and granule cell layer (GCL), and representation of the main cell types and fibers of the cerebellar cortex (modified from van der Heijden & Sillitoe, 2021).

The structural organization of the cerebellar cortex can be clearly observed in parasagittal histological sections of the *vermis* from adult mice, where, moving from the deepest to the most superficial layers, we can see: the white matter, containing the deep cerebellar nuclei; a densely packed internal granular layer, containing tightly packed cells; the thin Purkinje cell layer, composed of large cells arranged in a monolayer in mice; and the molecular layer, surrounded by the meninges (**Figure 7**) (Schröder et al., 2020).

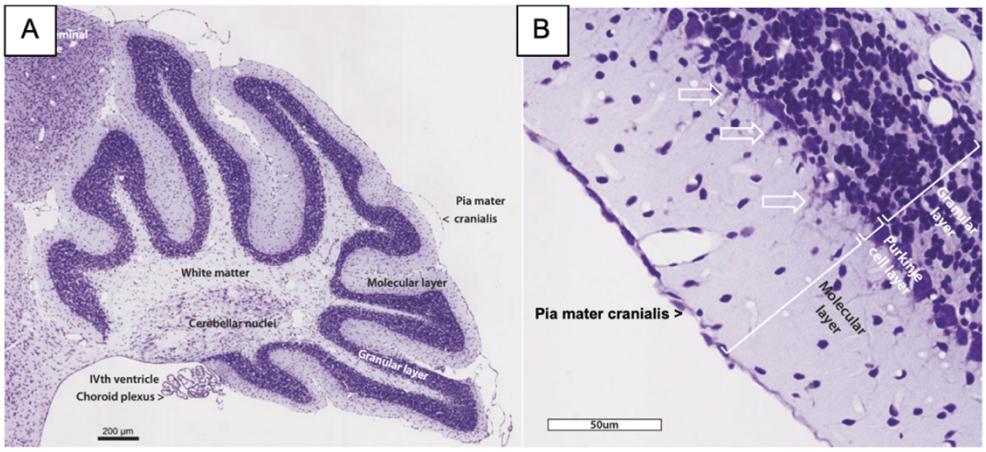

Figure 7. Parasagittal sections of a mouse cerebellum: **A**) the white matter, with the deep cerebellar nuclei, is located in the centre, bordered by the dense granule layer; at the bottom, the choroid plexus of the IV ventricle can be observed. **B**) Molecular layer, Purkinje layer and granular layer can be easily distinguished: the granule layer contains densely packed cells; the Purkinje layer is thin and contains large, pear-shaped Purkinje cells; the molecular layer is a cell-poor sheet lined by the pia mater cranialis (modified from Schröder et al.,, 2020).

1.1.2.1.The internal granule layer

The deepest layer of the cerebellar cortex is the *internal granule layer* which contains small (about 6 µm of diameter) and very densely packed granule cells; this internal cortical layer also includes some Golgi, Lungaro and unipolar brush (UBCs) cells. Excitatory granule cells are the most abundant neurons of the cerebellar cortex, accounting for 99% of the whole neuronal content of the cerebellum; these cells project their unmyelinated axons into the molecular layer, giving rise to the parallel fibers.

Golgi cells are inhibitory cells characterized by a large soma; some of these cells extend their dendritic tree in the molecular layer where they receive inputs from parallel fibers. Lungaro cells are inhibitory cells that share connections with each other as well as with Golgi cells and basket cells. Unipolar brush cells, conversely, are excitatory cells described in several mammalian species, including rodents; these cells are found in the vestibulocerebellum and

presumably provide a feedforward excitation signal to granule cells, determining enhanced inputs from the vestibular nuclei (Butler & Hodos, 2005).

Mossy fibers, which originate in the brainstem nuclei and spinal cord, are one of the main inputs to the cerebellum and terminate in the internal granule layer; these fibers excite directly granules cells through synaptic complexes called *cerebellar glomeruli*, which contain the inhibitory feedbacks from Golgi cells (Consalez et al., 2021). The core structure of the glomeruli are the *rosettes*, large grape-like terminals formed by the mossy fibers axons in the internal granule layer, Golgi neurons' terminals and granule cells dendrites (Sillitoe et al., 2012).

1.1.2.2.The Purkinje cell layer

Located between the internal granule layer and the molecular layer is the Purkinje cell layer, which constitutes the principal output of the cerebellum. It is composed by the large inhibitory Purkinje cells, organized in a single sheet in mice (Consalez et al., 2021). Purkinje cells (PCs) are named after Jan Evangelista Purkyně, the Czech physiologist who described them for the first time in the 19th century. In most mammals, including mice, Purkinje cells have a pear-shaped soma and, in sagittal sections of the cerebellar cortex, they exhibit a vast dendritic tree, which extends towards the outmost molecular layer (**Figure 8**); conversely, in coronal sections their dendritic tree appears less evident and more flattened. PCs slender axons, which extend from the opposite pole (bottom) of the cell, carry the major output of the cerebellum, releasing GABA transmitter towards the cells in the deep cerebellar nuclei or to the vestibular nuclei of the brain stem (Butler & Hodos, 2005).

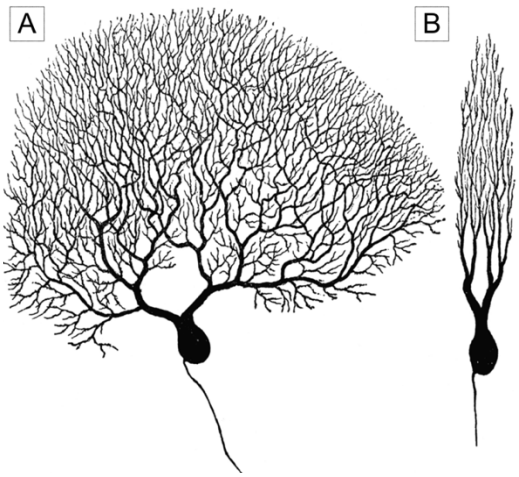

Figure 8. Schematic representation of a Purkinje cell: Purkinje cells have a large pear-shaped soma and, in sagittal view, the dendritic tree appears extended and branched (A), while in coronal view, it appears much more reduced and flattened (B) (modified from Florida Center for Instructional Technology).

1.1.2.3.The molecular layer

The most external layer of the cerebellar cortex is the molecular layer, a cell-poor sheet that contains the unmyelinated axons of the granule cells, the long dendrites of the Purkinje cells, and the soma and dendrites of the molecular layer interneurons (MLI), basket and stellate cells. MLIs are distributed throughout the molecular layer with and innervate Purkinje cells, with a typical pattern: basket cells, located in the lower half of the layer, have numerous dendrites and an axon that travels parallely to the Purkinje cells and sends descending collaterals; conversely, stellate cells occupy the upper half and their axons send ascending and descending collaterals to Purkinje cells.

This layer also contains the axons of granule cells, which run parallel to the *foliae* of the cerebellar cortex and are thereby named 'parallel fibers'. The climbing fibers are also present in this layer: they originate in the inferior olivary nucleus, in the brain stem, and wrap around the dendrites of Purkinje cells conveying sensory information from the periphery and cerebral cortex to the cerebellum (Kandel, 2021).

1.1.3. Glial cells

The great anatomical and functional complexity of the cerebellum is also corroborated by the presence of non-neural glial cells, which show high morphological and functional heterogeneity: microglia, oligodendrocytes and astrocytes. Glial cells contribute to the development and correct functioning of the CNS, and in the cerebellum they are classified into three categories, based on their morphology and localization: (i) glial cells of the white matter (including, fibrous astrocytes and oligodendrocytes), and (ii) velate protoplasmic astrocytes and (iii) Bergman glial (BG) cells, in the cerebellar cortex (Buffo & Rossi, 2013). Microglial cells, the immune system of the CNS, distribute both in white matter and in the cortex of the cerebellum. Additionally, microglia support oligodendrocytes development and play crucial roles in shaping neuronal circuits by regulating neurite growth, synaptic pruning; specifically, in the cerebellum they modulates synaptic pruning, eliminating excess climbing fibers and maintain a balanced GABA inhibition on PCs (Revuelta et al., 2020).

In the cerebellum, astrocytes are fundamental factors, contributing to overall tissue homeostasis; cerebellar astrocytes are located both in the cortical layers (BG cells and velate protoplasmic astrocytes) and in the white matter (fibrous astrocytes) (**Figure 9**).

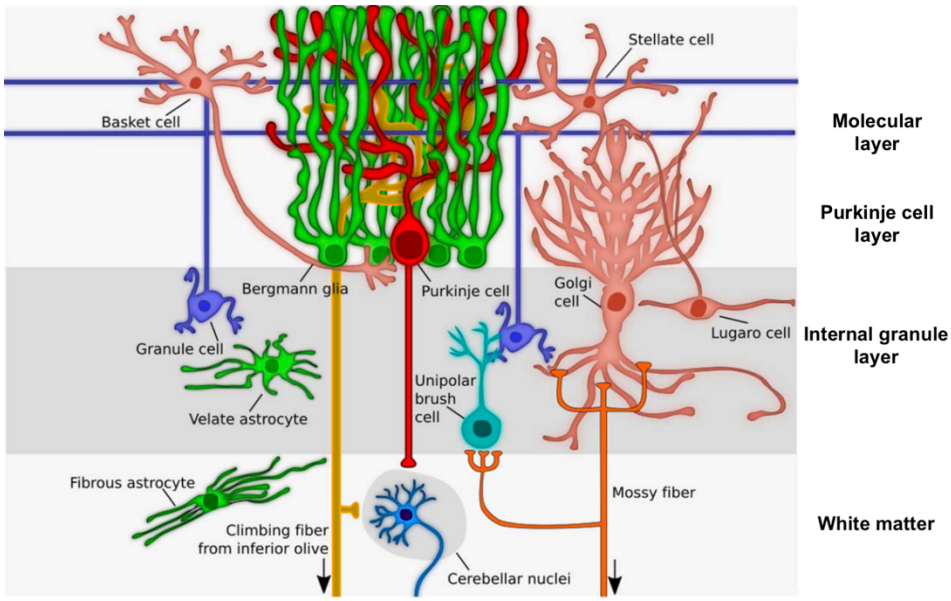

Figure 9. Schematic representation of cerebellar astrocytes: fibrous astrocytes, located in the white matter; velate protoplasmic astrocytes, located in the internal granule layer; Bergmann cells,with the soma located in the molecular layer and their projections spanning from the molecular layer to the Purkinje layer (modified from Carulli et al., 2020).

In the cerebellar cortex, velate protoplasmic astrocytes are located in the internal granule layer astrocytes interact with the *glomeruli*, suggesting they may support circuit functioning; fibrous astrocytes make extensibe contact with blood vessels; BG cells, originally known as Golgi epithelial cells, regulate cerebellar development and synaptogenesis (Carulli et al., 2020). BG cells are the most studied cerebellar astrocytes; they sre specialised astrocytes, derived from radial glial and their soma is located between the internal granule layer and the Purkinje layer, while their chandelier-like processes run through the Purkinje and molecular layer (Sillitoe et al., 2012). BG cells participate in several specific functions in the cerebellum, ranging from the modulation of cerebellar development and corticogenesis to the regulation of synaptic signaling at Purkinje cells (Cerrato, 2020).

1.1.4. Histogenesis and development of the cerebellum

The cerebellum originates from the roof of the rhombencephalon, one of the main divisions of the vertebrates' brains. The primary partitions of the cerebellum are the *corpus cerebelli* and the cerebellar auricle, and they consist of an outer layer (cerebellar cortex) and an internal white matter. The mature cerebellum is organized into three layers, each containing functionally specialised cells (Purkinje cells, basket and stellate interneurons, and granule cells). The histogenesis of the cerebellar architecture is a complex process: the largest neurons of the

cerebellum (the Purkinje cells) and the interneurons of the cerebellum are generated near the IV ventricle of the brain stem. After completing the final mitotic division, Purkinje neurons migrate radially and accumulate forming an irregular layer (the cerebellar plate). Conversely, the granule cells are generated from the rhombic lip, a different progenitor zone located at the rim of the IV ventricle.

During nervous system development, the shape and structure of tissues, cell bodies, dendrites, and axons must be precisely regulated to form intricately organized mature structures. This process requires a series of complex and balanced steps: the proliferation and differentiation of progenitor cells, migration, and ultimately, the establishment of connections between different structures (Long & Huttner, 2019). A key step for the development of all CNS structures is the migratory process; indeed, the correct spatial and temporal pattern in which neuronal migration takes place is of crucial importance for the correct functionality of neuronal circuits. The mouse cerebellum displays a neurodevelopmental very similar to that of the cerebral cortex. The developmental process of the cerebellum spans from embryonic to post-natal phases. The bilateral cerebellar primordium (CbP) appears at embryonic day 12.5 (E 12.5); the caudal mesencephalon forms to the anteromedial CbP, while rhombomere 1 gives rise to the posterolateral CbP. By E 15.5 it transforms into a smooth structure with a cylindrical shape that envelops the posterior parts of the brain. The folding of the mouse cerebellum takes place during the first two weeks after birth, during which it also subdivides into the three main cerebellar structures: the *central vermis*, the *lateral hemispheres* and the *paraflocculi* (Sgaier et al., 2005).

Aside from the definition of gross tissue morphology, another key event in both the CNS and cerebellar development is the neurogenesis and neuronal migration, which ultimately lead to the correct localization of cells and the formation of NS circuitries. The cerebellum has a complex and highly compartmentalized cytoarchitecture, which makes its circuits the most complex of all CNS structures. Therefore, the neurogenesis and migration of cerebellar neural and glial cells are intricate processes that cover both embryonic and postnatal periods. The excitatory and inhibitory cells of the cerebellum arise from germinally distinct neuroepithelia: the ventricular zone (VZ) for the inhibitory neurons, and the rostral rhombic lip (RL) for the excitatory neurons. The VZ in sequential waves gives rise to the Purkinje, Golgi, stellate and basket cells, as well as glial cells; the RL, situated at the boundary between the dorsal r1 and the roof of the fourth ventricle, generates the granule cells and the unipolar brush cells (Rahimi-Balaei et al., 2018).

After their final mitotic division between E10.5 and 12.5, Purkinje cells begin migrating radially along the radial glial fibers from the VZ to their final location in the cerebellar cortex. Purkinje cells axonogenesis occurs at E12.5 and by E14.5 they irregularly accumulate in a thick immature Purkinje cell layer; their projections towards the cerebral cortex do not start before E16 in mice. Between E18 and P3 Purkinje cells complete their maturation and start clustering. The precursors of stellate and basket cells inhibitory interneurons are generated by the VZ and subsequently migrate radially and accumulate at the borders of the external granule layer and finally reach the molecular layer. Similarly originating in the cerebellar plate ventricular zone, Golgi cells continue to proliferate while migrating until the perinatal period. Their migration concludes postnatally once they reach their final location in the granule layer. (Rahimi-Balaei et al., 2018).

Generated from the RL, between E12.5 and E17, granule cell precursors start migrating tangentially from r1 over the cerebellar plate and then constitute the external germinal zone, where they proliferate; subsequently, thanks to Bergman glial cells, postmitotic granule cells migrate radially past the Purkinje cells layer and ultimately form the granule layer in the first two weeks after birth. Between E13.5 and early perinatal period, also unipolar brush cells are also generated by the RL, migrate through the cerebellar white matter and ultimately locate in the granule layer (Rahimi-Balaei et al., 2018).

1.1.5. Cerebellar circuitry

The basic circuity of the mouse cerebellum is composed of both extrinsic and intrinsic connectivity, which are common to most vertebrates (**Figure 10**). The laminae of the cerebellar cortex envelop a core of white matter containing both afferent and efferent axonal pathways; these allow connections to several other regions of the CNS including the brainstem, the cerebral cortex, and the spinal cord. Several reciprocal connections to different areas of the cerebral cortex, such as the *motor area*, the *prefrontal cortex*, and the *temporal lobe*, constitute cerebro-cerebellar connection (Prati et al., 2024).

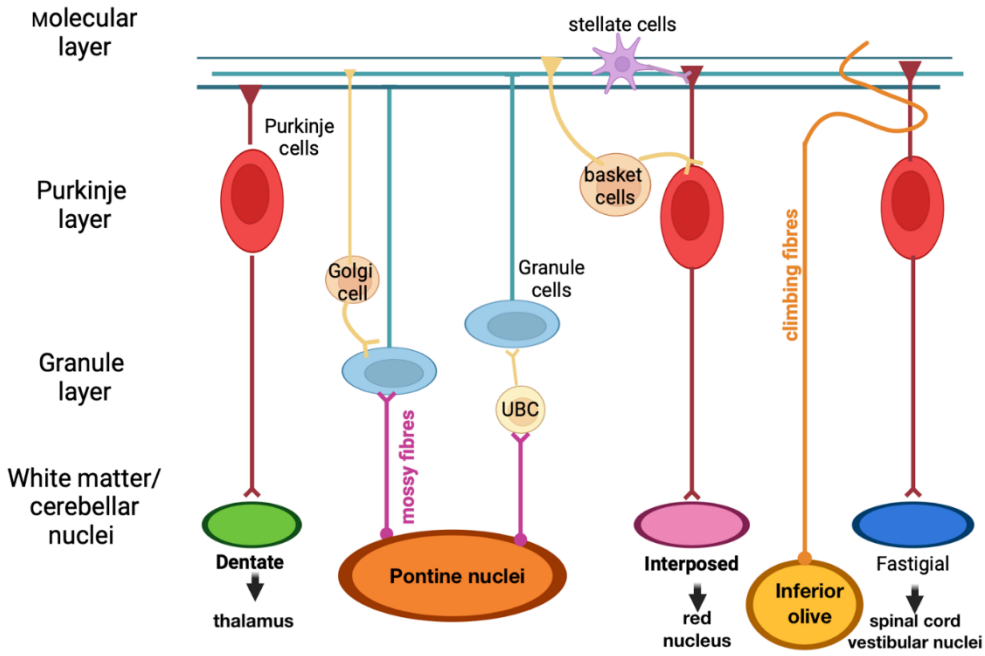

Figure 10. Schematic representation of the basic circuitry of the cerebellum: climbing fibers directly synapse Purkinje cells; mossy fibers interact with granule cells (either directly or through UBCs) and Purkinje cells. Granule cells are inhibited by Golgi cells; Purkinje cells are contacted by stellate and basket cells: the former reach Purkinje neurons dendrites, while the latter contact Purkinje cells soma and dendrites (modified from Consalez et al., 2021).

In mammals, the cerebellum receives inputs related to movement, coordination, and balance. Its afferents arise from the cerebral cortex, spinal cord, vestibular nerve, red nucleus, and tectum. The cerebellum is connected to the rest of the brain through three penducles: the superior (alternatively named *brachium conjunctivum*), the middle (or *brachium pontis*), and the inferior cerebellar peduncle (or *corpus restiforme*). The superior peduncle carries the ascending efferents to the red nucleus and dorsal thalamus as well as the afferent fibers of the spinocerebellar tract, which convey information from the lower spinal cord; the middle cerebellar peduncle is the most prominent source of afferent projections to the cerebellum from the pontine nuclei; the inferior peduncle contains both afferent (from the inferior olivary nucleus and spinocerebellar tract) and efferent fibers (to the vestibular nuclei) (Kandel, 2021). Inputs that reach the cerebellum through the cerebellar peduncles synapse the deep cerebellar nuclei and the cerebellar cortex, which facilitate movements and control movement the adjustment/refinement, respectively. Afferent projections arrive at the cerebellum through mossy fibers and climbing fibers. In particular, mossy fibers excite (either directly or through UBCs) granule cells, whose axons form the parallel fibers of the molecular layer and parallel fibers excite the dendrites of Purkinje cells and basket cells, parallelly, climbing fibers directly

excite Purkinje cells, literally climbing up their dendritic tree. In turn, excited Purkinje cells inhibit deep nuclei, constituting the cerebellar output (Butler & Hodos, 2005) and the deep cerebellar nuclei integrate the inhibitory inputs from the Purkinje cells with the excitatory inputs coming from mossy and climbing fibers. Mossy fibers comprise axons from vestibular nuclei, spinal cord, and pontine (in particular the reticular formation, which conveys inputs from the motor cortex) while climbing fibers relay inputs from the inferior olivary nucleus. Other afferents to the cerebellum arrive from multiple cerebral structures, e.g. hypothalamus, Raphe nuclei, and inhibitory signals from the locus coeruleus (Reeber et al., 2013).

The intrinsic connectivity of the cerebellum accounts for its inhibitory pathways, relayed by the cerebellar interneurons: stellate, basket, and Golgi cells. Stellate and basket cells inhibit Purkinje cells: the former only contact the dendrites, while the latter target both dendrites and soma; Golgi cells modulate the activity of granule cells (Consalez et al., 2021).

1.1.6. Cerebellar functions

Despite being considered the main CNS region involved in motor coordination and balance, the cerebellum plays both motor and nonmotor functions. In addition to motor control, movement planning and execution, the cerebellum also plays fundamental roles in vestibular functions, eye movement, as wel as cognitive and executive functions (such as working memory, attention processing and decision-making). Moreover, several neuropsychiatric conditions, e.g. schizophrenia, psychosis, autism-like behaviours and chronic pain, are linked to abnormal functionality of the *vermis* (Fujita et al., 2020). Task-related fMRI analyses have highlighted that motor and nonmotor cerebellar functions have an asymmetrical and compartmentalised organization resembling that of the cerebrum (**Figure 11**). The *anterior lobe* of the cerebellum plays an active role in motor functions. Language and working memory are primarily associated with strong activation in the right lobules, while visuospatial functions tend to be localized in the left hemisphere. Executive functions, on the other hand, are found in both hemispheres. The midline region of the cerebellum is mostly involved in behavioral and affective functions, thereby representing the so-called ‘limbic cerebellum’ (Klein et al., 2016). Recent research has

supported the non-motor roles of the cerebellum not only in humans but also in non-human species such as in rodents (Shipman & Green, 2020).

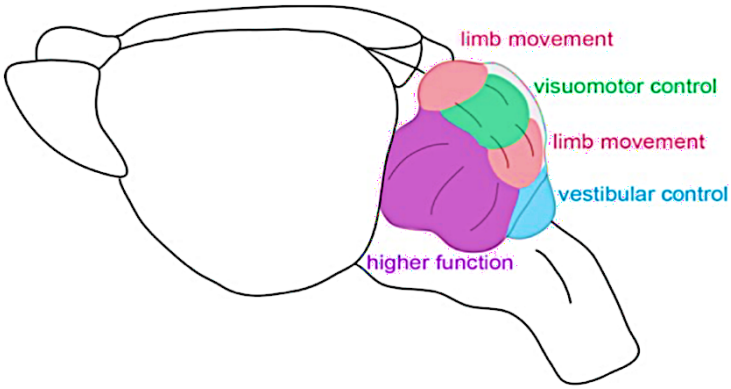

Figure 11. Compartmentalised distribution of motor and nonmotor functions of the murine cerebellum (modified from Reeber et al., 2013).

The primary role of the cerebellum is the direct control of movements and their refinement; the cerebellum is also involved in motor learning and reflex modulation; lesions to the cerebellum result in impaired gait and sensory control. Indeed, the cerebellum is fundamental for sensorimotor integration: through sensory feedback from receptors located in muscles, tendons, connective tissue, and skin, it can compare the former motor plan with the actual execution of an action, allowing correction of goal-directed movements. Moreover, the cerebellum contributes to the creation of "internal models" of the body, to enhance prediction and movement control: several sites of synaptic plasticity are present in the cerebellar microcircuit both in the cortex and deep nuclei. Given the substantial changes in activity observed during motor learning, the cerebellum has been proposed to participate actively in motor skill learning: the cerebellar motor learning theory states that the activity from the climbing fibers to the Purkinje cells can induce changes, particularly long-term depression (LTP), to the synapses between parallel fibers and Purkinje cells. However, in rodents, blocking LTP does not prevent motor learning, suggesting the involvement of other neuronal mechanisms (Kandel, 2021).

In mice, the cerebellum is closely connected to the vestibular nuclei and the reticular formation, allowing it to regulate balance and stabilize gaze during movement. Specifically, the vestibulocerebellum and spinocerebellum work together to process sensory information from the vestibular nuclei, helping to control posture, orientation, and balance. From there, signals are sent down to the spinal cord, triggering unconscious postural postural adjustments. Moreover, the spinocerebellum plays a complementary role to the basal ganglia in controlling

and adjusting posture: the former is involved in adaptations based on previous experiences, whereas the latter allows quick and immediate postural adjustments (Kandel, 2021).

The unipolar brush cells located in the *flocculonodular lobe* are fundamental for the vestibular functions of the cerebellum; this cerebellar neurons are categorised into two groups, working in tandem to finely modulate the vestibular inputs to the mossy fibers: (i) "ON brush cells" receive primary vestibular signals, while (ii) "OFF brush cells" are targeted by secondary vestibular afferents. Efferent pathways from the *flocculonodular lobe* extend back to the vestibular nuclei (Prati et al., 2024).

The cerebellum play a key role in the modulation and optimization of eye movements, enhancing visual performances; different cerebellar structures subtend several visuomotor functions, i.e. gaze-shifting, gaze-holding, gaze stabilisation, saccadic adaptation and target pursuit (Beh et al., 2017). Consequently, alterations in the physiological cerebellar structure or function are usually associated with the on set of nystagmus and diplopia (Patel & Zee, 2015). In mice, the vestibulocerebellum is crucial for phase control of compensatory eye movements: vestibulo-ocular reflexes (VOR) adaptation requires the communication between Purkinje cells of the *flocculonodular lobe* and the neurons of the vestibular nuclei (De Zeeuw et al., 1998).

Cognition is a major outcome of cerebral cortex activity, more specifically it is linked to the prefrontal cortex, but several studies have now highlighted extensive cerebellar implications in cognitive, affective and executive function. The cerebellum plays a critical role in cognitive processing, sensory discrimination, and emotional processing. Several fMRI studies allowed to map motor and cognitive functions, which display a medial-to-lateral cerebellar distribution in the cerebellum: while the sensory and motor functions are located medially, the cognitive functions are primarily distributed in the lateral portion of the neocerebellum and dentate nuclei. Connections between the cerebellum and the hippocampus through multiple pathways have been reported in murin model; in this respect, the cerebellum interacts with ventrolateral and laterodorsal thalamic nuclei to regulate seizure inhibition (Prati et al., 2024).

Moreover, recent studies have demonstrated the role played by the cerebellum in emotional processing, social behaviours and affective functions; indeed, the *vermis* and *fastigial nucleus* show interactions with limbic structures, such as the *amygdala* and *cingulate gyrus*: in the mouse, affective functions are regulated through the interactions between the fastigial nucleus and cerebral cortex, while *amygdala* and *cerebellar vermis* connections modulates emotional processes such as long-term fear memory consolidation. In the mouse fastigial nucleus, output neurons of the *vermis* where analysed through single-cell gene expression profiling and

neuronal tracing investigations; different subtypes of fastigial glutamatergic cells where discovered, each connected with Purkinje cells and neurons of the inferior olivary, which in turn project to several other station: these results unveil cerebellar disynaptic pathways not only with the basal ganglia but also with the basal forebrain and cerebral cortex, potentially responsible for the affective and cognitive functions of the *cerebellar vermis* ((Fujita et al., 2020). Additionally, anatomical tracing analyses revealed disynaptic connections between the *cerebellar vermis* and the *basolateral amygdala*, supporting a putative role of the cerebellum in emotional processes (Jung et al., 2022).Studies on murin spinocerebellar ataxia models have investigated the role of the cerebellum in cognition and mood; SCA2 mice suffer from spatial memory decline, anxiety and depressive-like symptoms, supporting an active role of the cerebellum in cognitive and affective functions, as well as conceivably in emotional processing (Marinina et al., 2024).

In rodents, executive functions are similar to those observed in humans; executive functions are classified as working spatial memory, attention, and decision-making. Cerebellar alterations in mice lead to cognitive flexibility and spatial navigation disfunctions. Studies on transgenic mice bearing specific cerebellar dysfunctions have highlighted the potential role of the cerebellum in working memory and spatial navigation: (i) mice carrying a mutation in the ionotropic glutamatergic receptor expressed by Purkinje cells show working memory impairments when tested with the radial-arm maze test; (ii) mutant mice affected by substantial Purkinje cells degeneration, and followed by secondary inferior olivary neurons degeneration, exhibit working memory deficits during delayed alternation tests; (ii) impairments in the long-term depression between parallel fibers and Purkinje cells, a form of cerebellar synaptic plasticity, may subtend for spatial navigation deficits. This collection of evidence suggests putative roles played by the mouse cerebellum in non-motor cognitive functions (Shipman & Green, 2020).

1.2. Osteogenesis imperfecta

Osteogenesis imperfecta (OI), or *brittle bone disease*, is the most common form of hereditary bone fragility, affecting both men and women, with an incidence of 1 in 15,000-20,000 newborns (Jovanovic et al., 2021). OI is a rare congenital connective tissue disorder linked to collagen defects and commonly known for its skeletal implications: e.g., reduced bone density, increased bone weakness and fracture risk, progressive skeletal deformity, such as mild facial dysmorphisms and macrocephaly. Parallelly to the well-known bone abnormalities, the disease also affects other connective tissues and causes several extraskeletal manifestations including

blue sclera, alterated tooth development, hearing loss as well as abnormal function of cardio-respiratory system (Yu et al., 2023).

Clinical symptoms, severity of disease and life expectancy vary greatly due to the high genetic heterogeneity of the disease regarding the type and position of the mutation, as well as the genetic background of the patient. Signs and symptoms range from mild to extremely severe. In particular, adults affected by this disease cope with a broad spectrum of symptoms: musculoskeletal and joint dysfunctions (e.g. muscle weakness, hypotonia and joint hyperflexibility), chronic pain, kidney stones, hearing and vision-related problems; a wide range of manifestations are observed in children as well: physical growth delays, scoliosis, progressive long bone deformities, and dental abnormalities (Zaripova & Khusainova, 2020). Additionally, childer affected by OI display early and marked delays in motor development and significant impairments in locomotor functions (Engelbert et al., 2000; Coêlho et al., 2021).

To date no specific treatment for OI has been developed: the pharmacological strategies currently available are only osteoporosis-approved drugs, which merely aid in managing the symptoms by increasing bone mass. In this regard, anti-reabsorption bisphosphonates (BPs) are commonly used in OI treatment: these drug inhibit osteoclasts activities, reducing the rate of bone reabsorption and consequently increasing bone mass (Alcorta-Sevillano et al., 2022).

1.2.1. Pathophysiology and genetics

The unifying hallmark of osteogenesis imperfecta is the direct involvement of collagen: it is often referred to as a collagen-related disorder of connective tissues, caused by defects in collagen structure, folding, post-translational modification and processing which ultimately result in defects in bone mineralization and osteoblast differentiation. OI is mainly linked to qualitative and quantitative defects of collagen type I, which is the prototypical collagen fibre and a key component of the extracellular matrix (ECM) of all body tissues. Therefore, alterations affecting this protein greatly compromise ECM structure, signalling and homeostasis (Jovanovic et al., 2021).

Collagen is the most abundant protein in mammals, accounting for approximately 25% of the total protein content. It is a structural protein and a core component of connective tissues such as skin, muscles, bones, cartilage, and teeth. To date, at least 29 different types of collagen have been described and classified into three groups based on their ability to form fibrils (Shenoy et al., 2022). The fibrillary structure of collagen is composed of three parallel, left-handed polyproline type II helices (α helices) forming a right-handed bundle. Its stable structure

endows collagen fibers with mechanical properties, high thermal stability, and the ability to form specific interactions with other molecules. The tight packing that characterizes collagens triple helix requires a glycine residue for every three amino acids, resulting in a sequence of Xaa-Yaa-Gly repeats. These repeats are present in all collagen types and the glycine residue in the Xaa-Yaa-Gly repeats is conserved, because the small side chain of glycine can be easily accommodated within the central axis of the left-handed α helices (**Figure 12**) (Wallace et al., 2011). Therefore, substitutions of glycine residues can result in disruptive modification of collagen structure and proper folding (Shoulders & Raines, 2009).

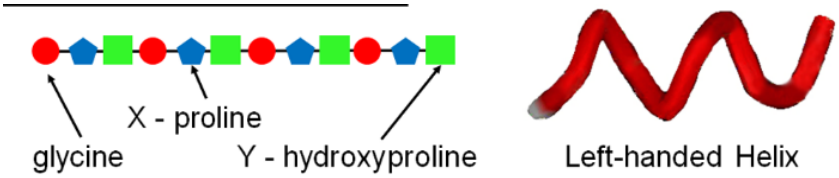

Figure 12. Molecular structure of collagen (modified from Wallace et al., 2011).

Collagen type I is synthesized as a procollagen type I molecule, a heterodimer composed of two α1 chains and one α2 chain and comprised of N-propeptides and C-propeptides. The α chains are generated and self-associate in the rough endoplasmic reticulum (RER), where they undergo post-translational modifications (Lv et al., 2022). Procollagen type I is transported to the Golgi apparatus and released by exocytosis into the ECM, where ADAMTS-2 and BMP1 enzymes proteolytically cleave the N- and C-terminal propeptides determining mature type I collagen to be integrated into the ECM (**Figure 13**) (Jovanovic et al., 2021). Collagen type I molecules are covalently cross-linked and packed into dense fibrils, granting mechanical and structural properties to virtually all connective tissues (bone, skin, joints, cartilage and cornea) (Ricard-Blum, 2011).

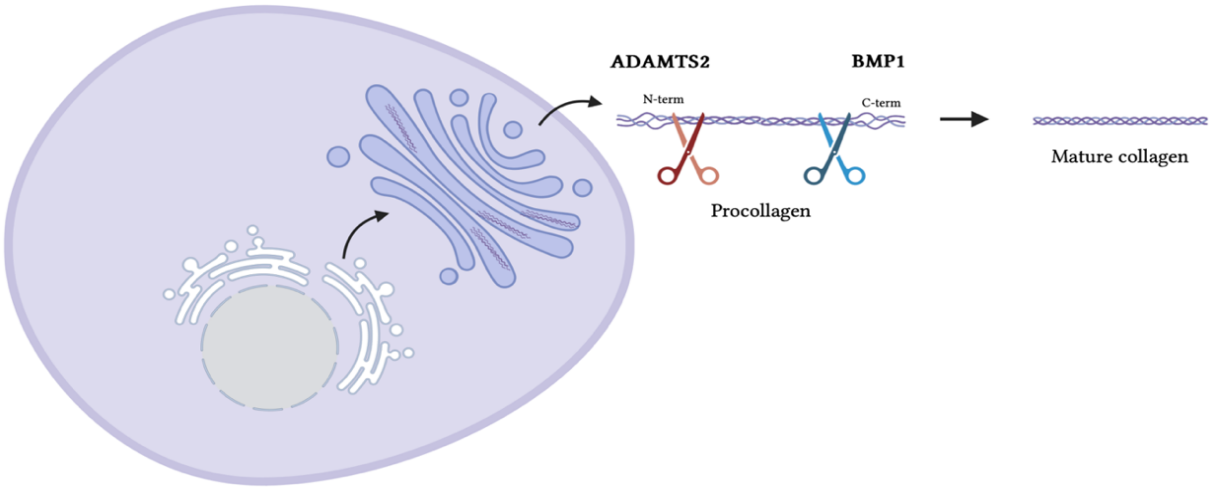

Figure 13. Schematic representation of collagen maturation process (created with BioRender.com).

OI is a genetically heterogeneous disease; qualitative and quantitative defects in collagen type I include: collagen type I decreased transcription, reduced secretion due to ER retention, alterations of post-translational modifications and abnormal propeptide processing or cross-linking. To date, at least 20 different mutations have been linked to OI onset and their inheritance modality covers autosomal dominant, autosomal recessive and X-linked recessive mutations. Pathogenic variants in *collagen type 1 alpha 1* (*Col1a1*) or *alpha 2* (*Col1a2*) genes, encoding collagen type I chains, are inherited in an autosomal dominant manner while variants in genes involved in synthesis and maturation of collagen can result in recessive forms OI (Nicol et al., 2021).

Most OI cases (over 80%) result from dominant mutations located in the *Col1a1* and *Col1a2* genes, which code for the α1 and α2 chains of type I collagen respectively (Yu et al., 2023). Substitutions occurring in the α1 chain often lead to a more severe and lethal phenotype: haploinsufficiency of *Col1a1* in humans results in a mild form of the disease, while haploinsufficiency of *Col1a2* results in a normal phenotype. Homozygous null α2 mutations result in manifestations from severe OI to a mild Ehlers-Danlos syndrome-like disorder (Lv et al., 2022). Non-sense mutations, shift mutations and splice mutations in *Col1a1* determine a reduced amount of type I collagen production and are associated with milder phenotypes, whereas SNPs (missense) mutations in *Col1a1* and *Col1a2* involving glycine residue substitution, that change collagen folding and structure, are often associated with severe pathology. Mutations in these genes have two possible outcomes: the formation of aberrant

collagen chains (qualitative mutations) or, more commonly, decreased collagen expression levels (quantitative mutations) (Steiner & Basel, 1993).

Replacement of glycine residues in α1 or α2 chains strongly destabilizes collagen structure and the degree of destabilization is linked to the type of amino acidic substitution, which in turn reflects on the severity of the disease. In particular, substitutions with either alanine or serine demonstrate a slight effect on both the conformation and stability of collagen, thereby contributing to a milder pathology, whereas substitutions with valine, aspartate, glutamate, or arginine are often associated with fatal OI; moreover, the extent of destabilization varies according to the position of the mutation. Most glycine replacements reported in the literature involve serine and cysteine substitutions (Nadyrshina et al., 2022). In addition to the mutations affecting type I collagen chains, several other rare causative genes affecting collagen folding and processing, bone mineralization and osteoblast differentiation have been discovered, making OI a collagen-related disease (Jovanovic et al., 2021). Less than 10% of OI patients display recessive mutations in genes involved in the synthesis and post-translational modification and cellular processing of type I collagen (e.g., *P3H1*, *CRTAP* and *BMP1*), in genes related to differentiation and mineralization osteoclasts (e.g., *IFITM5*) and in other non-collagenous proteins such as WNT1 (Nadyrshina et al., 2022). Other rare mutations associated with fewer OI cases involve KDELR2 and CCDC134 proteins. KDELR2 is a receptor family that is located in the endoplasmic reticulum and mutated isoforms of this protein are associated with mislocalization or reduction in HSP47 levels, a chaperon molecule involved in the correct maturation of collagen protofibrils in the ER; CCDC134 is a kinase that participates to the regulation of mitogen-activated protein kinase (MAPK): loss of function mutations in the gene encoding for this protein are associated with altered ERK1/2 phosphorylation and subsequent reduction in *Col1a1* expression.

The primary repercussion of the modified collagen structure is linked to the altered or missing engagement with ECM components thereby affecting ECM homeostasis and function, which ultimately dictates most of the phenotypic features associated with OI. In phisiological conditions, the network between collagen and ECM not only provides structural integrity to the tissue but is also linked to the wide range of signaling pathways, due to the role of ECM in orchestrating different cellular mechanisms. Collagen engages with several binding partners forming the *collagen interconnectome* with ECM constituents (such as fibronectin, heparin and proteoglycans), cell-surface receptors and, during turnover, with several matrix metalloproteinases (MMP) (Wareham et al., 2024). Other than the abnormal interaction with

ECM components, a potential pathogenic feature of mutated type I collagen is the induction of ER stress. Mutated collagen molecules are often subjected to abnormal cellular trafficking and to ER retention, which causes excessive modifications of the peptides and delayed secretion, leading to potential accumulation of misfolded collagen or selective deletion. Studies have highlighted increased expression of ER stress-related proteins in osteoblasts of OI-lethal mice (Jovanovic et al., 2021). Conceivably, ER stress can dictate cellular stress and trigger unfolded protein response (UPR), autophagy, and apoptosis (Bini et al., 2021). Variants in proteins involved in the modulation of the cytoskeleton (such as nestin), as well as non–collagenous components of the ECM (such as decorin), might correlate to the severity of the pathology (Bini et al., 2021).

1.2.2. Classification

Given the high genetic heterogeneity, several OI classifications have been proposed, all accounting for the great variability both within and between types (Yu et al., 2023). The original Sillence classification (1979) was based on clinical and radiological features, severity of symptoms and inheritance patterns and accounts for four different types of OI: OI type I (autosomal dominant) is the most common form, characterized by mild symptomatology with blue sclerae; OI type II is the fetal perinatal form; OI type III is severe and progressively deforming; OI type IV accounts for moderate-severity sings with normal sclera (Zaripova & Khusainova, 2020). These four classes are known as *classical OI types* and are all genetically linked to quantitative or qualitative mutations in *Col1a1* and *Col1a2* genes. OI type I, the milder form, is caused by one non-functional *Col1a1* allele, which determines the presence of only half of the normal amount of collagen (quantitative mutations); OI types II-IV display a more critical phenotype, linked to structural defects of collagen (qualitative mutations) often due to glycine substitutions (Bianchi et al., 2012).

In 2000, F.H. Glorieux, considering the advancements of molecular genetic studies, proposed an expanded classification with four more types of OI, not exclusively linked to type I collagen, accounting for 8 OI types (I-VIII). In 2016, the International Committee of Nomenclature of Constitutional Disorders of the Skeleton proposed a new classification of OI into five groups, including an additional OI type to the four classes originally individuated by Sillence (**Table 1**) (Zaripova & Khusainova, 2020). This modern classification accounts for the clinical manifestations, genetic and molecular features and the pattern of inheritance, providing a better

diagnosis and stratification of patients and paving the way for future therapeutic research (Yu et al., 2023).

Table 1 Modern classification of osteogenesis imperfecta (modified from Zariprova & Khusainova, 2020).

Type	Type name	Gene	Inheritance type
I	Non-deforming type with blue sclera	*COL1A1, COL1A2, SP7, BMP1, P3H1, PLS3*	AD, X-linked
II	Perinatally fatal, severe	*COL1A1, COL1A2, CRTAP, P3H1, CREB3L1, PPIB, BMP1*	AD, AR
III	Progressively deforming, moderately severe	*COL1A1, COL1A2, BMP1, CRTAP, FKBP10, P3H1, PLOD2, PPIB, SERPINF1, SERPINH1, TMEM38B, WNT1, CREB3L1, FAM46A*	AD, AR
IV	Variable OI with blue sclera, medium heavy	*COL1A1, COL1A2, WNT1, CRTAP, PPIB, SP7, PLS3, TMEM38B, FKBP10, SPARC*	AD, AR, X-linked
V	Moderate OI with ossification of the interosseous membrane of the forearm	*IFITM5*	AD

Note. AD is an autosomal dominant type of inheritance; AR is an autosomal recessive type of inheritance.

1.2.3. The role of collagen in the central nervous system

The physiological role of the ECM appears evident considering its evolutionary age: a key step in the transition from unicellular to pluricellular organisms was indeed the emergence of genes coding for ECM components (Wareham et al., 2024). Specifically, the ECM in the central nervous system (CNS) is not merely a passive scaffold providing mechanical support: accounting for approximately 20% of the whole brain mass, the ECM plays a biologically active role not only granting structural stability and mechanical properties but also governing the production and availability of signalling molecules: the ECM acts as a reservoir of several molecules, such as cytokines and growth factors, key molecules involved in cell adhesion, differentiation, migration and survival (Martins et al., 2021). The temporal and spatial regulation of ECM constituents throughout neurodevelopment drives neurogenesis, neuronal differentiation and migration, axonal growth and guidance. The ECM establishes a complex interplay between cells and integrates dynamically with neuronal and glial cells. Neurons, astrocytes, and microglial cells release several molecules essential for ECM maintenance and integrity: ECM reorganization drives synaptic plasticity throughout CNS development. Remarkably, brain-specific aggregates of ECM components surround the soma and dendrites of mature neurons in the CNS; these specialised lattice-like aggregates constitute the so-called perineuronal nets (PNNs), which support and stabilise synaptic connections and modulate neuronal plasticity. Formed by assemblies of proteins and carbohydrates, PNNs are abundant in several regions of the mammalians' brain, including the cerebral cortex, the hippocampus,

as well as the cerebellum. The deep cerebellar nuclei are particularly enriched in PNNs, where they regulate brain functions such as motor learning and memory: literature data indicates that PNNs depletion severely impacts cerebellar motor learning (Carulli et al., 2020). Particularly, PNNs regulate the synaptic contacts between PCs and the glutamatergic neurons of the deep cerebellar nuclei. Therefore, PNNs modulate processes such as the delay eye blinking conditioning, a form of cerebellar-dependent associative learning that involves eyelid closure in response to a previously neutral conditionate stimulus when paired with an unconditioned stimulus; consequently, depletion of the PNNs has been proven to significantly impair cerebellar motor learning (Hirono et al., 2018).

Despite not representing their main constituents, studies indicate that collagens participate in the regulation of PNNs organization and function (Wareham et al., 2024). Additionally, the ECM plays a major but also complex role in shaping CNS development: ECM elements may have similar or opposing effects on different neighbouring cells. Through the interactions with receptors expressed on the cell surface, ECM components have been demonstrated to significantly impact the proliferation, differentiation, and migration of cerebellar neuronal cells as well as in the morphogenesis of the cerebellum itself. In the neurodevelopmental stages, meningeal cells, which form the meningeal layers that envelope the brain, express a vast array of ECM elements, including fibrillary collagens such as collagen type I, II, and IV (Wareham et al., 2024). Notably, studies indicate a strict temporal and spatial regulation of collagens and laminins during embryonic and perinatal periods that match the origin and migration of cerebellar Purkinje neurons (Sur et al., 2014). Moreover, in zebrafish, collagen type IV controls axonogenesis in cerebellar Purkinje cells (Takeuchi et al., 2015).

Given the extensive role played by the cerebellum in several different domains, abnormal neuronal migration in the cerebellum may result not only in motor disorders but also in a broad range of neurodevelopmental disorders in humans, such as autism spectrum disorder (ASD), attention-deficit hyperactivity disorders (ADHD), as well as intellectual disability (ID) and developmental dyslexia. Several studies indicate that abnormalities in cerebellar subregions, resulting from early damages or alterations in cerebellar development, can lead to the disruption of the normal cerebral-cerebellar circuitry, thereby resulting in a wide range of behavioral symptoms. Indeed, patients affected by neurodevelopmental disorders and displaying cerebellar abnormalities often present co-occurrence of early motor, sensory, cognitive, and emotional deficits (Stoodley, 2016).

Both in humans and mice, the presence of collagen in healthy adult brains indicates that, following neurodevelopment, several cell types, such as endothelial and vascular smooth muscle cells, astrocytes, oligodendrocytes, and meningeal cells continue to express collagen isoforms (**Table 2**). Collagen secretion oligodendrocytes contribute to healing after brain injury as well as during neuronal development; the latter is also supported by meningeal cells collagen expression (Wareham et al., 2024). Collagen is found in marginal areas of the mature nervous system (NS), mainly in three locations: the connective tissues associated with the central and peripheral nervous system, the basement membranes between the NS and other tissues, and the sensory endings. Multiple members of the collagen superfamily, particularly collagen type I, have been demonstrated to participate in the NS development, axonal guidance, and synaptogenesis, and in the terminal differentiation of Schwann cells. Collagen also plays an active role in defining brain architecture and during the development of peripheral nerves. In the meninges lining and protecting the CNS, the presence of collagen type I has been observed in the dense network of collagen fibers constituting the dura mater layer (Hubert et al., 2009). Collagen type I has also been associated with astrogliosis and scar formation. In normal conditions, collagen synthesis in CNS is reduced; following spinal cord injuries, pericytes and fibroblasts produce and release collagen type I in response to cytokines like transforming growth factor β (TGFβ): collagen type I drives astrocytes' activation and promotes scar-forming phenotype through integrin/N-cadherins signalling mechanisms (Neo & Tang, 2017).

Table 2 Roles of collagen isoforms in the CNS (modified from Wareham et al., 2024).

CNS compartment	Collagen isoforms	Function in CNS
CNS development	Collagen I, IV, IX, XVIII	Guides neuronal outgrowth, maturation, circuit formation and synaptogenesis
Brain meningeal basal lamina	Collagen I, III, IV	Protects meningeal layers of the brain
Vascular basal lamina	Collagen IV, VII, XVIII	Lines blood vessels forming the BBB
Perineuronal nets (PNNs)	Collagen XIX (IV in disease states)	Stabilises synapses

1.2.4. NS involvement and neurodevelopmental issues in OI

OI phenotype is characterized by skeletal malformations including craniofacial changes and neurocranial abnormalities, such as cranial vault abnormalities (macrocephaly and delayed closure of fontanelles), cranial flattening and basilar invaginations. Abnormalities in the neurocranial skeleton may alter brain morphology, affecting the nervous system functions (Husain et al., 2024). Literature data reported a direct effect of the disease on brain and spinal

cord structure, highlighting a strong alteration of the CNS in OI. Several cases corroborate this CNS alteration, reporting cerebellar displacement and hypoplasia in patients affected by the disease. The softer and weaker bones at the base of the skull determine basilar impression, an abnormality of the craniovertebral junction resulting from the upward displacement of the odontoid process into the foramen magnum, which leads to brainstem compression and obstruction of cerebrospinal fluid flow in the spinal canal (Khandanpour et al., 2012). Consequences of the craniocervical abnormalities are neurological impairments: trigeminal neuralgia, head an neck pain, as well as sleep disturbances have been reported in patients affected by OI (Arponen et al., 2018; Marulanda et al., 2024).

Furthermore, carotid-cavernous fistula and cerebral aneurysms, as well as susceptibility to spontaneous intracranial and extracranial hemorrhages reported in literature, highlight the involvement of the cerebrovascular system. Perivenous microcalcifications were also observed in the CNS of OI patients (Emery et al., 1999), likely caused by vascular collagen deposits, and enlarged perivascular spaces. Conceivably, the fragility of the neurovascular system is to be associated with abnormal collagen (Husain et al., 2024).

Similarly, brain parenchyma can be affected by the disease, e.g. cerebral atrophy and communicating hydrocephalus were shown in OI (Khandanpour et al., 2012). Neuropathological findings associated with defects in neuronal migration and alterations in the white matter of patients have been reported (Emery et al., 1999), and possible abnormalities in neuronal migrations and differentiation are supported by the presence of neural progenitor cells within white matter in the dysplasic areas (Verkh et al., 1995).

Children affected by OI frequently display developmental delays, especially in the more severe forms of the disease, but these issues exhibit mitigation with growth. Some neurodevelopmental delays, involving motor skills and speech, often arise due to forced immobilization to avoid fractures and, to some extent, to progressive hearing loss especially if present from an early age (Efthymiou et al., 2021). Several studies report hypotonia, muscle wearkness and early, marked delays in meeting motor milestones, such as sitting in an upright position or lifting the head in the prone position show reduced global motor function (Engelbert et al., 2000; Pavone et al., 2017). Moreover, different degrees of intellectual disability and cognitive impairment are reported in patients with loss-of-function mutations in *WNT1* gene (Etich et al., 2020). The protein encoded by this gene plays a key role in the WNT/β-catenin signaling pathway, which regulates osteoblast differentiation and bone regeneration and mutations in *WNT1* gene have been associated with neurological disorders in OI (Yu et al., 2023).

Moreover, some OI cases report psychiatric issues and seizures, although the occurrence rate of autism, hyperactivity and epilepsy is comparable to that of the general population. However, abnormal electroencephalogram (EEG) such as prominent photic driving responses (repetitive visual evoked potentials in response to photic light stimulations) and focal paroxysmal discharges occur unusually frequently in patients with OI (Juraški et al., , 2017).

1.3. Brtl *in vivo* model

In the last several years, the emergence of animal models for OI has improved our knowledge and understanding of OI molecular and pathological mechanisms. Mouse models are the most widely used OI animal models due to the similarity shared between humans and mice in underlying the genetic and pathological mechanisms of the disease (Bini et al., 2021).

Given the heterogeneity of the disease, several mouse models for OI are reported in the literature, carrying mutations (either naturally occurring or transgenically introduced) linked with collagen type I synthesis and processing. To date, several transgenic OI mice are available: (i) OIM, heterozygotic G610C Mice (Amish Mice), (ii) Brittle Mice (Brtl), (iii) Jrt Heterozygous Mice, Crtap Mouse, and (iv) IFITM5 Transgenic Mice. These *in vivo* models are used in preclinical research and they aim to reproduce the broad range of genetic and phenotypic hallmarks of OI: depending on the mutation, these mice display a wide range of symptoms and disease severities.

Among the most used *in vivo* models for OI is the Brtl mouse, which has been developed as the first knock-in model for OI. In particular, using the Cre/Lox system we may introduces a glycine to cysteine substitution at amino acid position 349 (G349C point mutation) into one *Col1a1* allele and produce the same pathological alteration observed in OI patients (Lv et al., 2022). This mutation has been demonstrated to be directly linked with altered collagen type I nanoscale morphology (Wallace et al., 2011). Both homozygous (Brtl/Brtl) and heterozygous (Brtl/+ or Brtl$^{+/-}$) mice are viable and the latter is frequently used to investigate classical OI since it well recapitulates the clinical features of dominant OI in humans, with the typical phenotypic variability found in OI patients. Interestingly, homozygous Brtl mice display a normal bone phenotype and reduced bone brittleness compared to Brtl/+, possibly due to a molecular mechanism that stabilizes all α1 collagen chains through disulfide bonds between cysteines (Jovanovic et al., 2021).

The heterozygous Brtl model, hereinafter referred to simply as Brtl, was developed to reproduce the moderately severe form of the disease (OI type IV) since G349C point mutation in *Col1a1*

is found in patients affected by OI IV (Blouin et al., 2019). Indeed, Brtl mice display the genetic and phenotypic hallmarks of type IV OI patients, characterized by severe skeletal alterations; such as bone fragility, reduced bone density and deformities. Moreover, this *in vivo* model also showed the molecular, biochemical, and radiographic features of OI patients, and thereby well recapitulates the clinical course and phenotype of OI patients, including short stature, increased bone fragility, and impaired remodelling (**Figure 14**) (Kozloff et al., 2004). Furthermore, ultrastructural studies in Brtl mice revealed that the mutant type I collagen fibers destabilize fibrils organization, which indeed appear thinner compared to the wildtype condition (Wallace et al., 2011). Evaluating cellular alterations, several studies reported cytoskeletal reorganization, ER stress, and autophagic abnormalities; indeed, altered expression of chaperon proteins, metabolic enzymes, and molecules involved in apoptotic pathways suggest impairments in several cellular functions and these alterations were not only found in bone tissues but also in skin and lung specimens of Brtl mice . Overall, the Brtl model displayed the same variability observed in human patients, both in pathophysiological and phenotypical terms, thereby posing as an excellent animal model for OI (Alcorta-Sevillano et al., 2022).

Figure 14. Phenotypic features of heterozygous Brtl murine model: the Brtl mutant appears significantly smaller compared to a wildtype mouse; Brtl mice also suffer from increased bone fragility, higher risk of fractures, and deformities (modified from Bianchi et al, 2012).

1.4. Oxidative stress

One of the main factors that can impact on tissue integrity and functionality is oxidative stress, which results from the excessive production of reactive oxygen species (ROS) and reactive nitrogen species (RNS) in response to different stimuli. These substances are detrimental to cells and neurons, leading to protein, lipids and nucleic acid damage. Normally resolved by the

activation of specific antioxidative systems within cells, oxidative stress can become an endogenous insult when these repair mechanisms are insufficient, determining an imbalance between the production and clearance of ROS and RNS. ECM and its remodeling process are rapidly affected by oxidative stress. DNA damage and ECM dysfunctions are tightly related: DNA damage in response to oxidative stress can induce several cellular changes such as ECM remodelling (**Figure 15**). Oxidative stress can promote the expression of ECM genes, including *Col1a1*, and excessive ROS production might exacerbate OI symptomatology, supporting the evidence that antioxidant drugs could prove beneficial. On the other hand, abnormalities in ECM constituents might themselves trigger oxidative stress and cause ROS-induced DNA damage (Martins et al., 2021). These findings hold significance, particularly for the diseases associated with alterations in extracellular matrix components, such as OI. Indeed, mitochondrial dysfunctionalities and increased ER stress reported in OI determine ROS overproduction and subsequent increases in oxidative stress levels, which may lead to cell damage. Notably, studies have highlighted that osteogenesis imperfecta mouse-models bearing collagen type I mutations have exhibited mitochondrial dysfunctions. Specifically, compared to controls, OI mice show a decreased expression of electron chain transport IV and cytochrome oxidase I, with the subsequent reduction of energy production. Moreover, collagen type I deficiency correlates with high ROS levels, which may also exacerbate OI symptomatology (Martins et al., 2021).

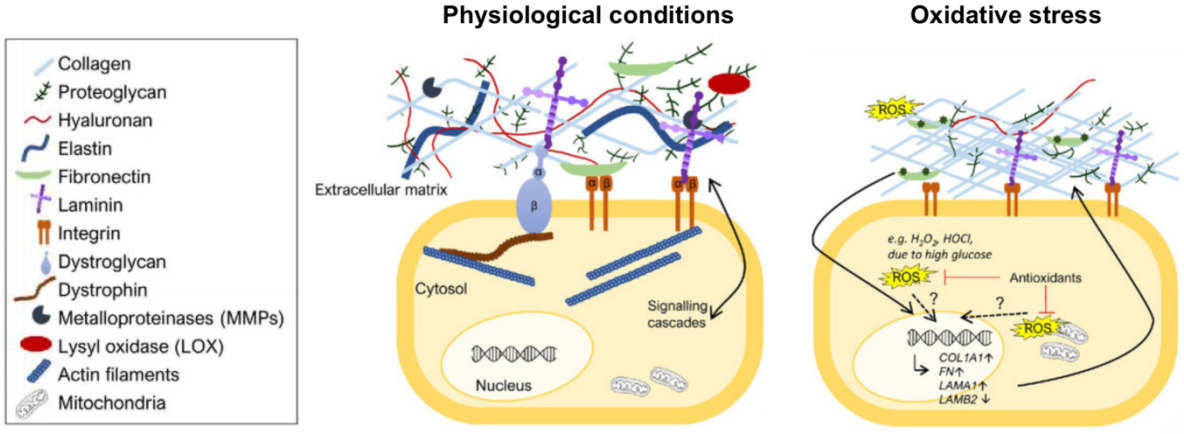

Figure 15. ROS-mediated DNA damage triggers ECM remodeling, increasing the expression of several ECM molecules, such as fibronectins, laminis and collagen, and the transcription of Col1a1 gene (modified from Martins et al., 2021).

The brain is particularly vulnerable to oxidative stress due to its high metabolic demand and its poor antioxidant capacities. Moreover, the brain is rich in phospholipids, which are particularly

prone to ROS-mediates peroxidation. Oxidative stress can lead neurons to hypoxia or hypoglycemia and, without sufficient oxygen, neuronal activity is impaired, therefore numerous studies have linked altered REDOX state to brain aging and neurodegenerative diseases such as Alzheimer's or Parkinson's diseases. Since the brain has a high rate of oxygen consumption, 20% of the whole organism's oxygen budget, it is strongly susceptible to oxidative stress, which can impair CNS activity.

1.4.1. NRF2

To cope with oxidative stress, cells upregulate their antioxidant systems, e.g., through the activation of the Nuclear factor erythroid 2-related factor 2 (NRF2), an oxidant and inflammation response transcription factor that plays a critical role in protecting cells from oxidative stress which causes tissue damage and inflammation. NRF2 is expressed in the CNS by neurons, astrocytes, and microglia to reduce cellular oxidative stress as well as glutamate-induced excitotoxicity (Song & Long, 2020). NRF2 regulation occurs at post-translational level through several mechanisms: by phosphorylation and by the action of the negative regulator Kelch-like ECH-associated protein 1 (KEAP1). The KEAP1-NRF2 pathway (**Figure 16**) is a crucial defence mechanism against oxidative stress. There are four essential components to this inducible pathway: (i) reactive chemicals that act as inducers of the system, (ii) KEAP1, an adaptor protein capable of binding to NRF2 and of sensing the inducer, (iii) NRF2, a transcription factor that activates the expression of antioxidant and detoxifying systems, and (iv) NRF2 target genes, which exert a protective role against oxidative stress. Under physiological conditions, NRF2 is located in the cytoplasm where it is maintained at low levels by KEAP1, which regulates NRF2 stability and proteasome-dependent degradation. Indeed, KEAP1 is an adaptor protein capable of binding NRF2 and forming an E3 ubiquitin ligase complex, the final actor in the protein ubiquitination process, thereby leading to NRF2 proteasome-dependent degradation. The presence of reactive cysteine residues makes KEAP1 oxidative stress sensor: when ROS levels increase, KEAP1 E3 ubiquitin ligase activity is inhibited. Consequently, NRF2 is released, phosphorylated and enters the nucleus, where it promotes the expression of NRF2-responsive genes by binding to the antioxidant response element (ARE). Therefore, the KEAP1-NRF2 system is responsible for the upregulation of the cellular antioxidant machinery, e.g., superoxide dismutases (SODs) and GPx4 (Baird & Yamamoto, 2020).

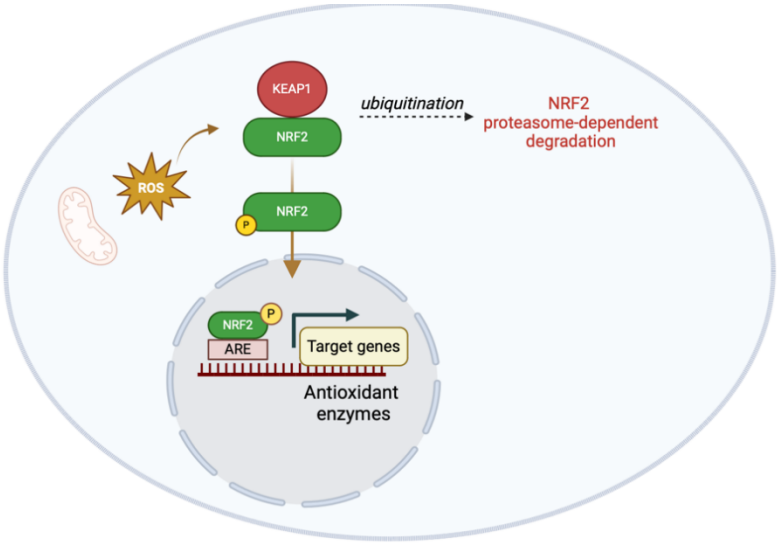

Figure 16. Schematic diagram of the KEAP1-NRF2 signalling pathway: under physiological conditions, KEAP1 mediated NRF2 ubiquitination and proteasome-dependent degradation; during ROS exposure, KEAP1 degradation is inactivated: NRF2 is phosphorylated and translocates into the nucleus where it binds to the ARE sequences and allows the transcription of genes encoding for antioxidant enzymes (created with BioRender.com).

1.4.2. SOD2

The superoxide dismutase family is a fundamental component of the antioxidant pathways and accounts for essential detoxifying agents. Present at different cellular locations, these proteins are metalloenzymes: by using metals as cofactors, they are responsible for the conversion of highly reactive superoxide radical anion ($O_2^{\bullet -}$) into hydrogen peroxide (H_2O_2), which is further reduced to water (H_2O) by catalase. The manganese-dependent superoxide dismutase 2 (SOD2) is located in the mitochondrial matrix: alongside with SOD1 and cytochrome c, both located in the intermembrane space), SOD2 reduces ROS production, thereby preventing oxidation of Kreb's cycle enzymes and maintaining redox balance (**Figure 17**). SOD2 is crucial for cellular development and homeostasis and substantial changes in SOD2 expression levels can result detrimental, leading to adaptive responses that can severely impact cell functionality; dysregulated SOD2 expression has been associated with numerous pathological states, including cancer, metabolic dysfunctions, and neurological disorders (Palma et al., 2020).

Since it plays such a crucial antioxidant role, during oxidative stress and inflammation, specific transcriptional factors translocate to the nucleus, bind SOD2 promoter and upregulate SOD2 expression, to cope with the redox imbalance (Fu et al., 2016). Specifically, in the CNS, SOD2

upregulation has been associated with increased oxidative damage in microglia cells, suggesting the role played by SOD2 in the antioxidant defences of the brain (Ishihara et al., 2015). Additionally, studies report an age-dependent regulation of SOD2 expression determining reduced levels of SOD2 in older subjects (Tatone et al., 2006), as well as decreased activity of this antioxidant enzyme, due to age-related increase in post-translational lysin acetylation (Fu et al., 2016); the downregulation of SOD2 protective function leads to accumulation of ROS and, consequently, supports the increase in oxidative damage (Díaz et al., 2024).

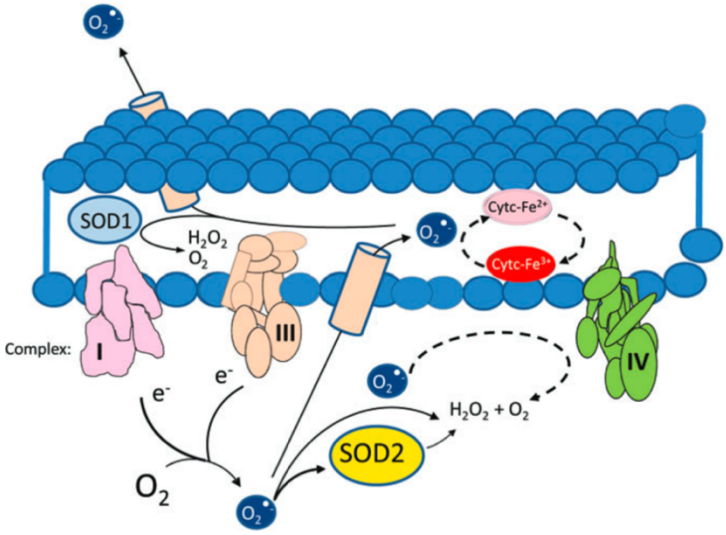

Figure 17. Schematic diagram representing the mitochondrial antioxidant machinery: cytochrome c, SOD1 and SOD2 enzymes work as protectors against the diffusion of ROS generated during the mitochondrial respiration; SOD2 is located in the mitochondrial matrix, where it catalyses the dismutation of the superoxide anion into hydrogen peroxide; SOD1 and cytochrome c are located in the intracellular space (modified from Palma et al., 2020).

1.4.3. GPx4

Glutathione peroxidases (GPx) are a family of antioxidant agents responsible for converting hydrogen peroxide to water. They constitute a crucial system for maintaining proper redox balance in mammalians. Currently, eight members of the GPx family are known (GPx1-8), each with specific sites of action and tissue distribution. GPx1-4 and GPx6 are selenium-containing GPx proteins, also known as selenoproteins; they contain selenocysteine in their catalytic system which enables them to reduce peroxides to less toxic compounds (Pei et al., 2023). In particular, GPx4 can also catalyse the reduction of lipid peroxides and is involved in the regulation of ferroptosis; ferroptosis, an iron-dependent form of cell death linked to

phospholipid peroxidation induced by oxidative stress, depends on the accumulation of a labile iron pool: iron can react with lipid-based ROS and, through Fenton reaction, lead to a peroxidative chain reaction. GPx4 uses the tripeptide glutathione (GSH) as electron donor substrate to reduce phospholipid hydroperoxides to alcohols; phospholipid hydroperoxides are produced by ROS and, in turn, interact with the redox-active ferrous iron (**Figure 18**) (Jiang et al., 2021). Since iron-catalysed propagation of ROS is responsible for the increase in oxidative stress, GPx4 plays a critical role in the regulation of membrane lipids peroxidation and the overall extent of cellular oxidative stress. GPx4 is expressed during neurodevelopment as well as in neuronal cells of adult mice, where it plays a key role in the homeostatic balance (Chen et al., 2015). Mitochondrial dysfunctions, possibly resulting from the increase in ROS levels, can lead to altered processing of GPx4. In this pathological condition, GPx4 can undergo a non-enzymatic and irreversible post-translational modification (PTM) named *succinylation* and mediated by fumarate. Indeed, accumulation of fumarate due to mitochondrial dysfunctions, may lead to an increase in PTM events that reduce the GPx4 functionality, further leading to an even higher increase in oxidative stress exacerbating cell damage (Cui et al., 2022).

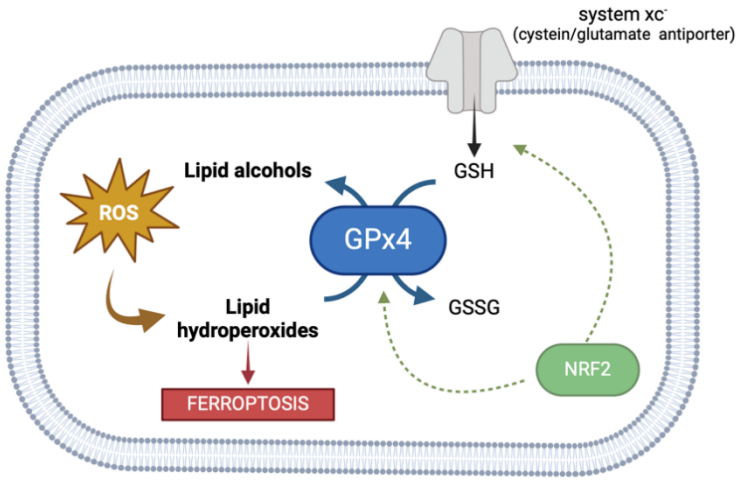

Figure 18. Schematic representation of GPx4 antioxidant activity: reactive lipid hydroperoxides produced by ROS are responsible for ferroptosis, a form of cell death. GPx4 enzyme catalyses the reduction of membrane-derived phospholipid hydroperoxides into phospholipid alcohols, using as cofactor reduced glutathione (GSH), which is oxidated into GSSG; GSH synthesis depends on the system xc^- antiporter (cysteine/glutamate antiporter). GPx4 and system xc^- antiporter expression can be regulated by NRF2 (created with BioRender.com).

1.4.4. COX4

Mammalian cytochrome c oxidase (COX), also known as complex IV, is a bigenomic, multisubunit enzyme formed by 13 subunits: 10 are encoded by nuclear DNA (COX4-13), while the remaining 3 are encoded by mitochondrial DNA (COX1-3) and form the functional core of the enzyme. COX complex works as a dimer and catalyses the final and rate-limiting step in the oxidative phosphorylation in mitochondria: it transfers electrons from cytochrome c to molecular oxygen, reducing the latter to water and preventing ROS generation (Sinkler et al., 2017). COX4 is the largest subunit of the complex encoded by nuclear DNA and is fundamental for proper mitochondrial respiration and ATP production; indeed, it appears to be critical for COX assembly and operates as a regulatory subunit of the complex, responsible for feedback inhibition of the enzyme's activity in response to high ATP concentration (Bikas et al., 2020). COX4 is present in two isoforms: (i) COX4-1 (encoded by *COXIV-1*), widely expressed in all mammalian tissues under physiological conditions, and (ii) COX4-2 (encoded by *COXIV-2*), suggested to enhance COX activity since it is mainly expressed under hypoxia and oxidative stress (Douiev et al., 2021). Low levels of molecular oxygen induce the expression of a transcription factor, hypoxia-inducing factor 1 (HIF-1), which modulates the switch between the two COX4 isoforms. Indeed, HIF-1, in turn, activates the transcription of *COXIV-2* and *LON*, a protease responsible for COX4-1 degradation. Moreover, also high ROS concentrations can act as signals and regulators of mitochondrial protein expression, e.g., assembly and synthesis of COX subunits, including COX4-2 (Bourens et al., 2013).

COX cooperates in the regulation of redox balance and COX4 deficiency, which leads to decreased COX activity and overall causes mitochondrial perturbations, is associated with ROS accumulation (Bikas et al., 2020); in turn, mitochondrial damage and mitochondrial DNA mutations act as apoptotic signals, therefore altered COX activity may trigger cell death. Particularly, in the brain COX4-1 expression appears to be crucial to synaptic functionality and neuronal networks activity: mutant mice knock-down for the COX4 subunits exhibit mitochondrial deficits that may subtend synaptic dysfunctions (i.e. reduction in synaptic markers density) and impaired neuronal network perturbations (Kriebel et al., 2020).

2. Aim

Osteogenesis imperfecta is a heterogeneous group of genetic disorders linked to collagen defects and primarily known for abnormal bone matrix deposition, which leads to bone fragility and growth impairments. On the other hand, collagens are crucial proteinic constituents of the extracellular matrix and play a vital role in several other tissues, making osteogenesis imperfecta a *connective tissue disorder*. OI patients display a wide spectrum of symptoms, both with skeletal and extraskeletal outcomes, including locomotor deficits. Based on these data, the purpose of the present thesis work is to evaluate the possible link between locomotor impairment observed in OI patients and the possible involvement of key CNS areas directly involved in the regulation/coordination of motor activity. Therefore, this study aimed to evaluate potential morphological changes and immunohistochemical alterations of oxidative stress pathway in the cerebellum of the Brtl mouse strain, a murine model for Osteogenesis imperfecta which carries a heterozygous mutation in the *Col1a1* gene. In particular, the presence of morphological alterations in the cerebellum of Brtl mice was evaluated using Hematoxylin-Eosin and Picrosirius Red stainings. Parallelly, the alteration of the oxidative stress pathway was analyzed by immunohistochemical reactions, investigating possible changes/modifications in the expression level of specific oxidative stress markers, i.e. (i) NRF2, (ii) SOD2, (iii) GPx4, and (iv) COX4.

3. Materials and methods

3.1. Mouse strain

This study used CD1/129Sv/B6 *Col1a1*$^{+/G349C}$ mice (Brtl), carrying a heterozygous G349C substitution in the *Col1a1* allele; wildtype littermates were used as controls. Mutant and control mice were maintained following standard experimental animal care protocols, in accordance with Italian Law, in the centralised animal facility of the University of Pavia (Italy). All experiments were approved by the OPBA (Body for the Protection of Animals) of the University of Pavia and by the Italian Ministry of Health (protocol n. 243/2018-PR, 27/03/18) and were performed according to EU Directive 2010/63/EU.

3.2. Cerebellar specimen preparation and experimental design

At the age of 18 months, mice were deeply anaesthetised by isoflurane inhalation before decapitation (Aldrich, Milwaukee, WI, USA). Cerebella were excised immediately after and then washed in 0.9% NaCl and then fixed by immersion in 4% paraformaldehyde in 0.1 M phosphate buffer (pH 7.4) for 7 hours. Tissues were dehydrated using an ascending graded ethanol scale followed by acetone and finally embedded in Paraplast X-TRA (Sigma Aldrich, Milan, Italy). Eight micrometre thick sagittal sections of *cerebellar vermis* were cut serially using a manual rotary microtome and collected on silane-coated slides.

Then, cerebellar tissues were processed for morphological and histochemical evaluations, using Haematoxylin and Eosin (H&E) staining and Picrosirius Red (PSR) staining. Immunohistochemical reactions were assessed to study possible modulation/alteration of the expression levels of specific oxidative stress markers.

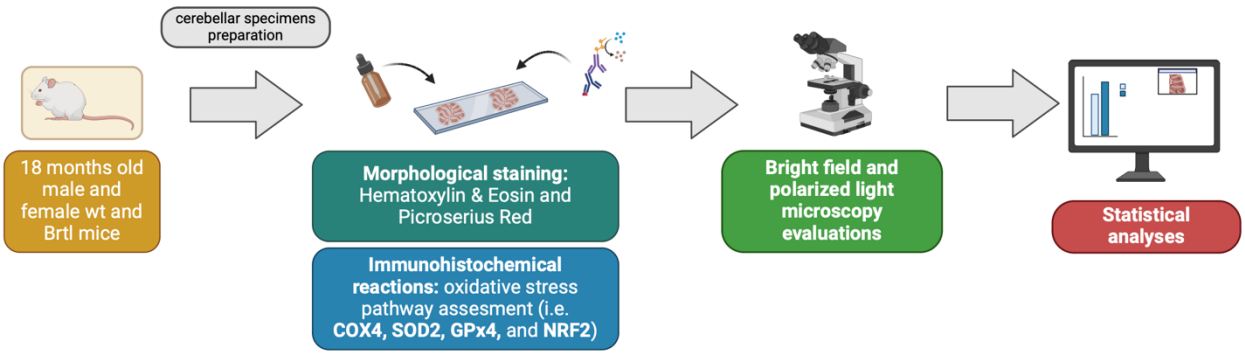

Figure 19. Experimenal flow chart (created with Biorender).

3.3. Histological stainings

H&E and Picrosirius Red stainings were performed to assess structural changes by bright-field microscopy. Cerebellar specimens of wildtype and Brtl mice were immersed in xylol for 10 minutes and rehydrated using a descending-graded ethanol scale. Subsequently, sections were stained according to the specific histological (histochemical and immunohistochemical) technique.

3.3.1. Haematoxylin and Eosin staining

Cerebellar slides were dipped into hematoxylin for 10 minutes and then washed with running water; subsequently, the sections were rapidly stained with eosin (30 seconds), washed in H_2O, dehydrated by ascending graded ethanol scale and cleared in xylene. Finally, the slides were mounted using Eukitt (Kindler gmbH) for bright-field microscopy evaluations.

3.3.2. Picrosirius Red staining

For collagen staining, rehydrated cerebellar sections were stained for 1 hour using Picrosirius Red solution (0.1% of Sirius red saturated in an aqueous picric acid solution). Then, the slides were washed in 5% acidified water, dehydrated in ethanol, cleared in xylene and mounted using Eukitt (Kindler gmbH).

3.4. Immunohistochemical reactions: oxidative stress assessment

Immunohistochemical assessments were carried out simultaneously on cerebellar slices from different experimental groups to avoid differences in staining caused by small procedural changes. Immunohistochemical reactions were performed using commercial antibodies on murine cerebellar sections to investigate the expression, localization, and distribution of specific markers of oxidative stress pathway: cytochrome c oxidase subunit 4 **(**COX4), superoxide dismutase 2 (SOD2), glutathione peroxidase 4 (GPX4), and nuclear factor erythroid 2–related factor 2 (NRF2).

Cerebellar sections of wildtype and Brtl mice were immersed in xylene for 10 minutes and rehydrated using the ascending graded ethanol scale; subsequently the sections were processed for immunohistochemical reactions. The slides were incubated overnight at room temperature in a dark moist chamber with monoclonal primary antibodies (**Table 3**) diluted in PBS. Then the slides were incubated with the respective biotinylated secondary antibodies (**Table 3**) for 1 hour and an avidin biotinylated horseradish peroxidase complex (Vector Laboratories,

Burlingame, CA, USA) was used to reveal the antigen/antibody interaction site. The 3,3′-diaminobenzidine (DAB) tetrahydrochloride peroxidase substrate (Sigma, St. Louis, MO, USA) was used as chromogen. Carazzi's hematoxylin was used to perform nuclear counterstaining.

Table 3. Primary and secondary antibodies and respective dilutions used for immunohistochemical reactions.

	ANTIGEN	MANUFACTURED AND SPECIES	DILUTION
Primary antibodies	**Anti-Glutathione Peroxidase 4 (GPx4)**	Abcam (Cambridge, MA, USA), Rabbit polyclonal IgG, Cat# ab231174	1:100
	Anti-Superoxide Dismutase-2 (SOD2)	Cell Signaling Technology (Danvers, MA, USA) Rabbit monoclonal IgG, Cat# 13141	1:200
	Nuclear factor erythroid 2-related factor 2 (NRF2)	Abcam (Cambridge, MA, USA), Rabbit polyclonal IgG, Cat# ab31163	1:200
	Cytochrome C Oxidase Subunit 4 (COX4)	Abcam (Cambridge, MA, USA) Mouse monoclonal IgG2a, Cat# ab14744	1:200
Secondary antibodies	**Biotinylated hoarse anti-mouse IgG**	Vector Laboratories (Burlingame, CA, USA), Horse, Cat# PK-6102	1:200
	Biotinylated goat anti-rabbit IgG	Vector Laboratories (Burlingame, CA, USA), Goat, Cat# PK-6101	1:200

3.5. Bright field microscopy

All sections were examined using bright field microscopy, with Leica DM6B WF microscope (Leica microsystems, Buccinasco, MI, Italy), and images were acquired with a Leica dfc 7000 t CCD camera (Leica microsystems, Buccinasco, MI, Italy). PSR-stained slices were also analysed under polarized light microscopy to discriminate the different maturation degrees of collagen fibers.

3.6. Histochemical and immunohistochemical evaluations

For each histochemical and immunohistochemical analysis, the evaluation was performed in 3 randomly chosen images/sections, with at least 10 measurements performed per image for 5 photographs/animal in each experimental group. In the figures are shown the most representative images for each experimental condition.

The extent of histological and immunohistochemical labellings were assessed on digitalized images of the cerebellar sections. Using densitometric analyses the intensity of the labelling was quantified with Image-J. The first step was to convert the picture in 8 bits and subsequently invert the colors of the image to obtain a light signal on a dark background, hence correlating the intensification of the immunopositivity with the increase in optical density; using the polygon selection (**Figure 20**) to ensure high accuracy of the area under analysis, the mask was adjusted depending on spatial distribution, signal localization and different layer or cell type. The intensity of the histochemical or immunohistochemical signal was measured as the mean of intensity value over the area and indicated as optical density (OD); immunopositive cells density count (number of immunopositive cells/area in mm^2) were also measured for a number of samples.

Figure 20. Polygon selections tool on Image-J.

3.7. Statistical analyses

Data were expressed as mean ± SEM. The D'Agostino & Pearson, Anderson–Darling, Kolmogorov–Smirnov and Shapiro–Wilk tests were performed to evaluate the normality distributions of data. Subsequently, collected results were processed to verify statistically significant differences. In particular, for results that did not pass the normality test, the analyses were conducted using the Mann-Witney test. Differently, for normally distributed data, the analysis was performed employing an Unpaired t-test. The differences were considered statistically significant for $p < 0.05$ (*), $p < 0.01$ (**) and $p < 0.001$ (***).

4. Results

4.1. Histological evaluations

Using Hematoxylin and Eosin (H&E) staining, morphological and cytoarchitectural characteristics of the cerebellar specimens were evaluated, by comparing male and female 18-months-old control (Ctrl) and Brtl mice. All sample groups display the typical three-layered structure of the cerebellar cortex, from outermost to innermost: molecular layer (ML), Purkinje cell layer (PCL) and granule layer (IGL), and indicate a well-preserved morphology and cytoarchitecture: the ML with few cells and rich in axons and fibers, the PC with large pear-shaped cells organized in a single row above the IGL, and the IGL with heavily stained nuclei of the small, densely packed cells. No gross morphological abnormalities were detected between the groups (**Figure 21**, **Micrographs A-H**).

However, the evaluation of ML and IGL cell densities between control and Brtl specimens revealed strong cerebellar cytoarchitectural differences between the evaluated experimental groups, with an ML and IGL cell density significantly reduced both in male and female Brtl animals, compared to control (**Figure 21**, **Panel a** and **Pabel b**, for ML and IGL cell density respectively; **Table 4**).

Picrosirius Red (PSR) staining was used to analyze collagen since it granted high-sensitivity visualization and quantification of collagen networks using bright field microscopy as well as polarized, allowing the discrimination between mature (green) and immature (red) fibers. In control and Brtl mice of both male and female mice, PSR positivity was localized in the meninges of the cerebellum, as well as in the choroid plexus of the IV ventricles (**Figure 22**).

Bright field microscopy highlighted a significant PSR OD decrease in the meninges of Brtl male animals, compared to control male mice (**Figure 23, Panel a** and **Panel b**, for meninges OD and choroid plexus OD, respectively; **Table 5**). A slight PSR labeling reduction was also observed in Brtl female animals, compared to female control group. Additionally, PSR stain was observed under polarized light to better discern between mature and immature collagen fibers (**Figure 2**, **Micrographs I-P**). Contrl and Brtl mice display well-defined mature and immature collagen fibers in the meninges and choroid plexus. Despite that, a highly significant reduction in both mature collagen fibers was revealed by quantitative analyses in the meninges and choroid plexus of male and female mutant mice (**Figure 23, Panels c** and **Panel e**, for the

meninges and choroid plexus, respectively; **Table 6**). Analogously, OD analyses also revealed a highly significant reduction in immature collagen fibers of male and female Brtl mice both in the meninges (**Figure 23, Panel d**; **Table 6**). On the other hand, female mutants also showed a highly significant reduction in immature collagen OD in the choroid plexus, while males displayed only a slight decrease in immature collagen fibers compared to the controls (**Figure 23, Panel f**; **Table 6**).

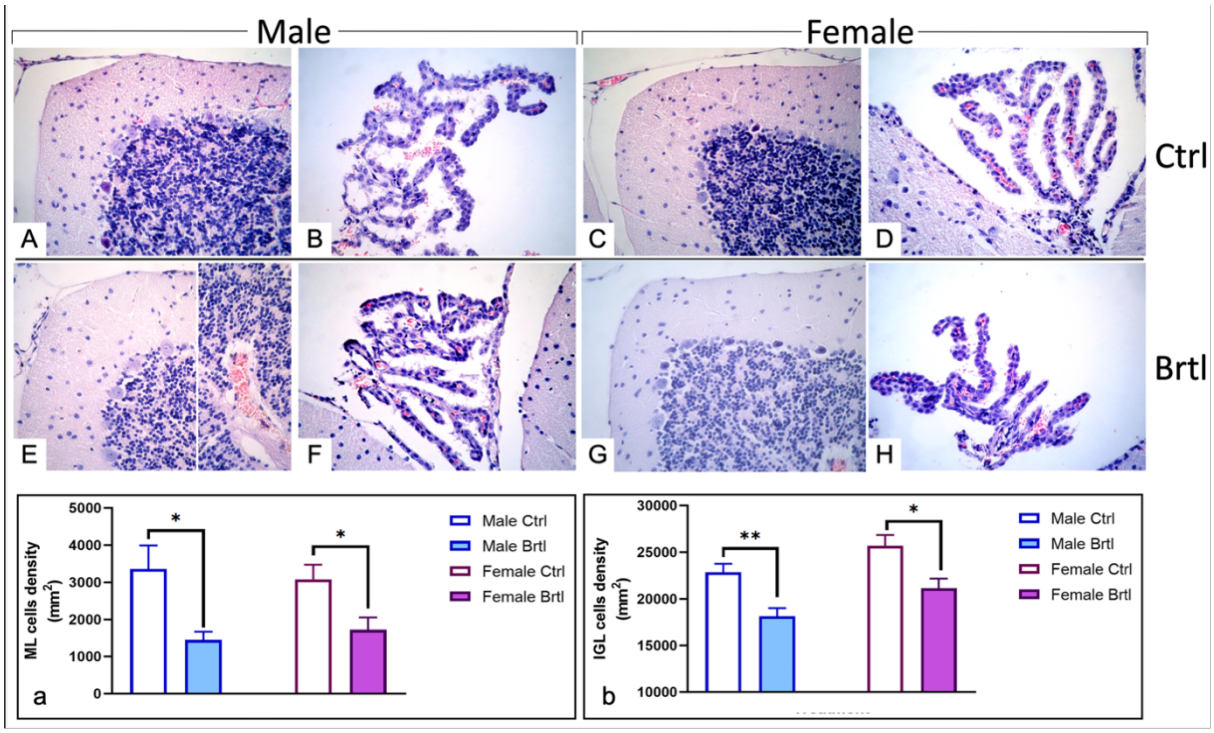

Figure 21. Representative H&E results showing cerebellar cortex (A, C, E, and G) and choroid plexus (B, D, F, and H), in male (A, B, E, F, and G) and female (C, D, H, and I) mice of control (A-D) and Brtl (E-I) groups. Microscopy magnification: 40× (A-E, G-I); 60× (F). Histograms (Panels A and B) show the quantitative measurements of the molecular layer (ML) and internal granule layer (IGL) cell density, respectively. p values: * $p < 0.05$; ** $p < 0.01$.

Table 4. Statistical analysis for the quantitative evaluation of quantitative evaluation of ML and IGL cell density. (*) $p<0.05$; (**) $p<0.01$.

	Experimental group		**Experimental group**	***p*-value**
ML cell density (n/mm²)	Male Ctrl (3358.90 ± 635.47)	*vs*	Male Brtl (1452,50 ± 222.37)	*
	Female Ctrl (3086.56 ± 390.46)	*vs*	Female Brtl (172.84 ± 333.55)	*
IGL cell density (n/mm²)	Male Ctrl (22876.86 ± 891.78)	*vs*	Male Brtl (18156.23 ± 861.23)	**
	Female Ctrl (25691.07 ± 1162.57)	*vs*	Female Brtl (21152.01 ± 1041.02)	*

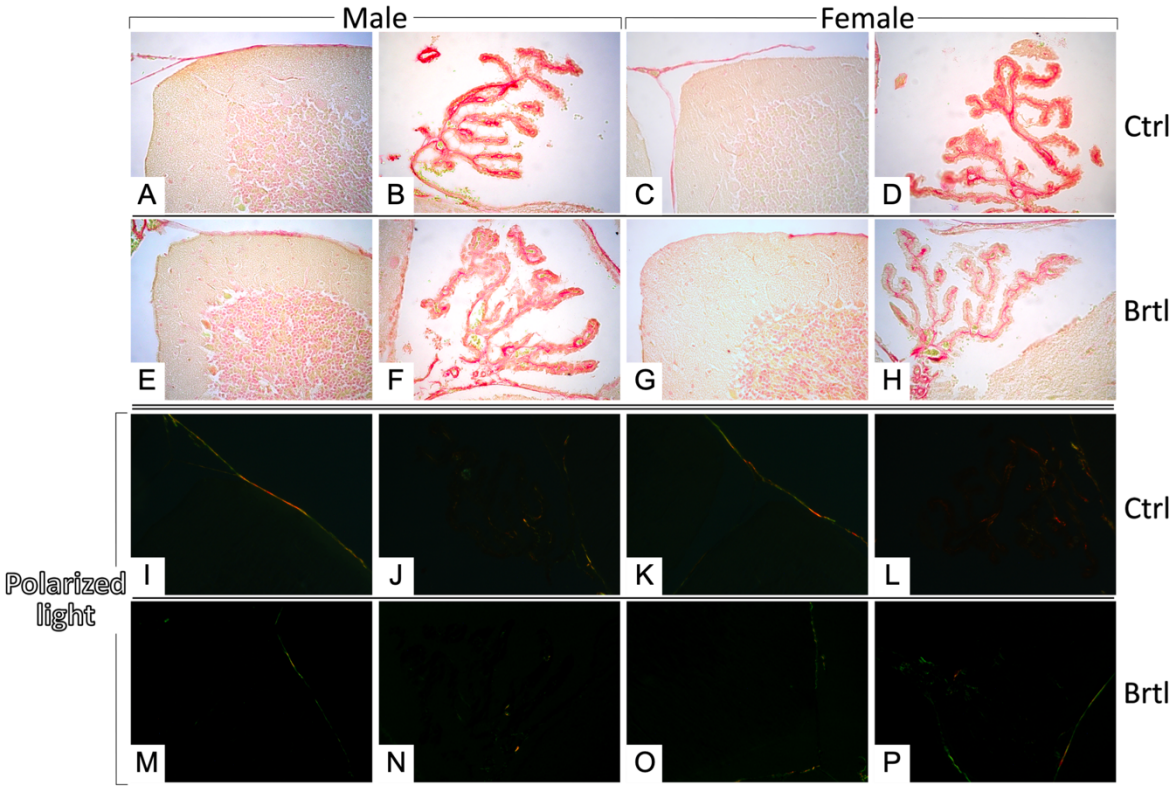

Figure 22. Representative PSR results showing cerebellar cortex (A, C, E, G, I, K, M, and O) and choroid plexus (B, D, F, H, J, L, N, and P) cerebellar slices, in male and female control (A-D and I-L) and Brtl (E-H and M-P) mice. Microscopy magnification: 40×. Micrographs A-H were obtained using bright field miscopy,while micrographs I-P under polarized light microscopy. Polarized light was used to discriminate between mature (green signal) and immature (green signal) collagen fibers.

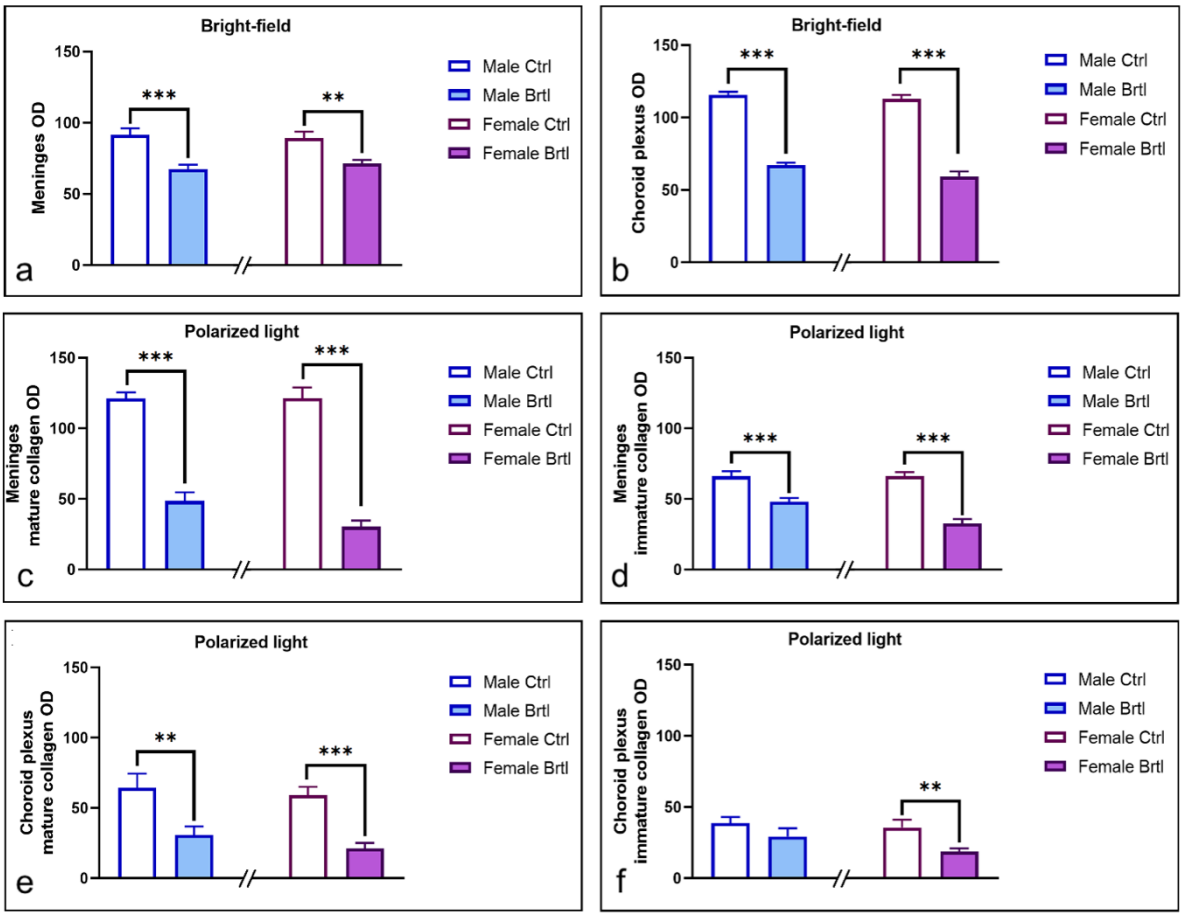

Figure 23. Histograms showing the quantitative measurements of meninges and choroid plexus optical density (OD) in male and female mice of the control and Brtl groups. Panels a and b: bright field PSR quantitative measurements in the meninges and choroid plexus, respectively. Panels c and d: polarized light PSR quantitative measurements of mature and immature collagen fibers, respectively, in the meninges. Panels e and f: polarized light PSR quantitative measurements of mature and immature collagen fibers, respectively, in the choroid plexus. p values: * $p < 0.05$; ** $p < 0.01$; *** $p < 0.001$.

Table 5. Statistical analysis for the quantitative evaluation of bright field PSR OD measurements in the meninges and choroid plexus. (**) p<0.01; (***) p<0.001.

	Experimental group		**Experimental group**	***p*-value**
OD measurements in meninges	Male Ctrl (91.58 ± 4.56)	*vs*	Male Brtl (67.50 ± 3.11)	***
	Female Ctrl (89.32 ± 4.52)	*vs*	Female Brtl (71.47 ± 2.46)	**
OD measurements in choroid plexus	Male Ctrl (115.53 ± 2.43)	*vs*	Male Brtl (67.00 ± 1.92)	***
	Female Ctrl (112.99 ± 2.67)	*vs*	Female Brtl (59.42 ± 3.44)	***

Table 6. Statistical analysis for the quantitative valuation of polarized light PSR mature and immature collagen OD measurements in meninges and choroid plexus. (ns) not significant; (**) p<0.01; (***) p<0.001.

	Experimental group		**Experimental group**	***p*-value**
Mature collagen OD measurements in meninges	Male Ctrl (121.18 ± 4.36)	*vs*	Male Brtl (48.55 ± 6.11)	***
	Female Ctrl (121.60 ± 7.50)	*vs*	Female Brtl (30.48 ± 4.26)	***
Immature collagen OD measurements in meninges	Male Ctrl (66.10 ± 3.53)	*vs*	Male Brtl (48.02 ± 2.70)	***
	Female Ctrl (66.13 ± 2.92)	vs	Female Brtl (32.68 ± 3.12)	***
Mature collagen OD measurements in choroid plexus	Male Ctrl (64.38 ± 10.05)	*vs*	Male Brtl (30.85 ± 6.09)	**
	Female Ctrl (59.14 ± 5.88)	*vs*	Female Brtl (21.15 ± 4.00)	***
Immature collagen OD measurements in choroid plexus	Male Ctrl (38.64 ± 4.43)	*vs*	Male Brtl (29.42 ± 5.59)	*Ns*
	Female Ctrl (35.73 ± 5.46)	*vs*	Female Brtl (18.72 2.38)	**

4.2. Oxidative stress pathway

Mutations in ECM components, such as collagen, can lead to aberrant ECM remodeling and have a detrimental impact on tissue homeostasis by increasing oxidative stress levels (Martins et al., 2021)..

COX4 is a component of the cytochrome c oxidase (COX) enzyme complex, or complex IV, thereby participating in the final steps of the mitochondrial oxidative phosphorylation (Bikas et al., 2020). **Figure 24** shows representative micrographs of COX4 immunostaining in the cerebellum of Brtl mice: a strong immunopositivity can be observed in the soma and dendrites of PCs, in the IGL mossy fiber rosettes, in the deep cerebellar nuclei and choroidal epithelial cells. Quantitative analyses evidenced a significant reduction in COX4 immunopositive OD in PCs and IGL mossy fiber rosettes (**Figure 25, Panel a** and **Panel c,** for PCs and IGL mossy fibers rosettes respectively) in mutants of both genders. However, only a minimal non-significan decrease of COX4 immunopositive Purkinje cells in male and female Brtl mice (**Figure 25, Panel b**). Contrarely, an extremely highly significant reduction of COX4 immunopositive OD was detected in the deep cerebellar nuclei of female mutants, and male mice exhibited a significant decrease as well (**Figure 25, Panel d**). Similarly, a significant reduction in COX4 immunopositive cells was detected in the deep cerebellar nuclei of male mutants and a highly significant increase was reported for female mutant mice (**Figure 25, Panel e**). On the other hand, COX4 immunopositive OD analyses revealed an extremely highly significant reduction in Brtl male mice and only a slight reduction in Brtl female mice (**Figure 25, Panel f**) (**Table 7**).

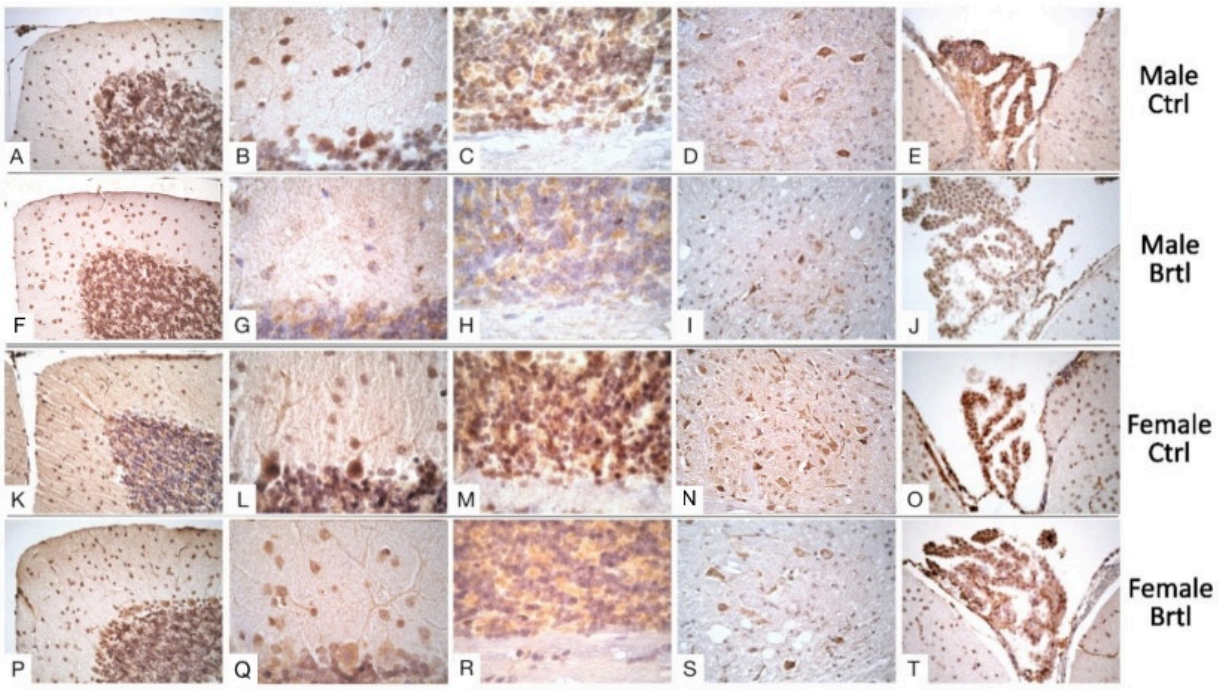

Figure 24. Representative results showing COX4 immunostaining in cerebellar cortex (A, B, C, F, G, H, K, L , M, P, Q and R), deep cerebellar nuclei (D, I, N and S), and choroid plexus (E, J, O and T) in control (A-E and K-O) and Brtl (F-J and P-T) cerebellar slices from male (A-J) and female (K-T) mice. Light microscopy magnification: 40 x (A, D, E, F, I, J, K, N, O, P, S and T); 60× (B, C, G, H, L, M, Q and R).

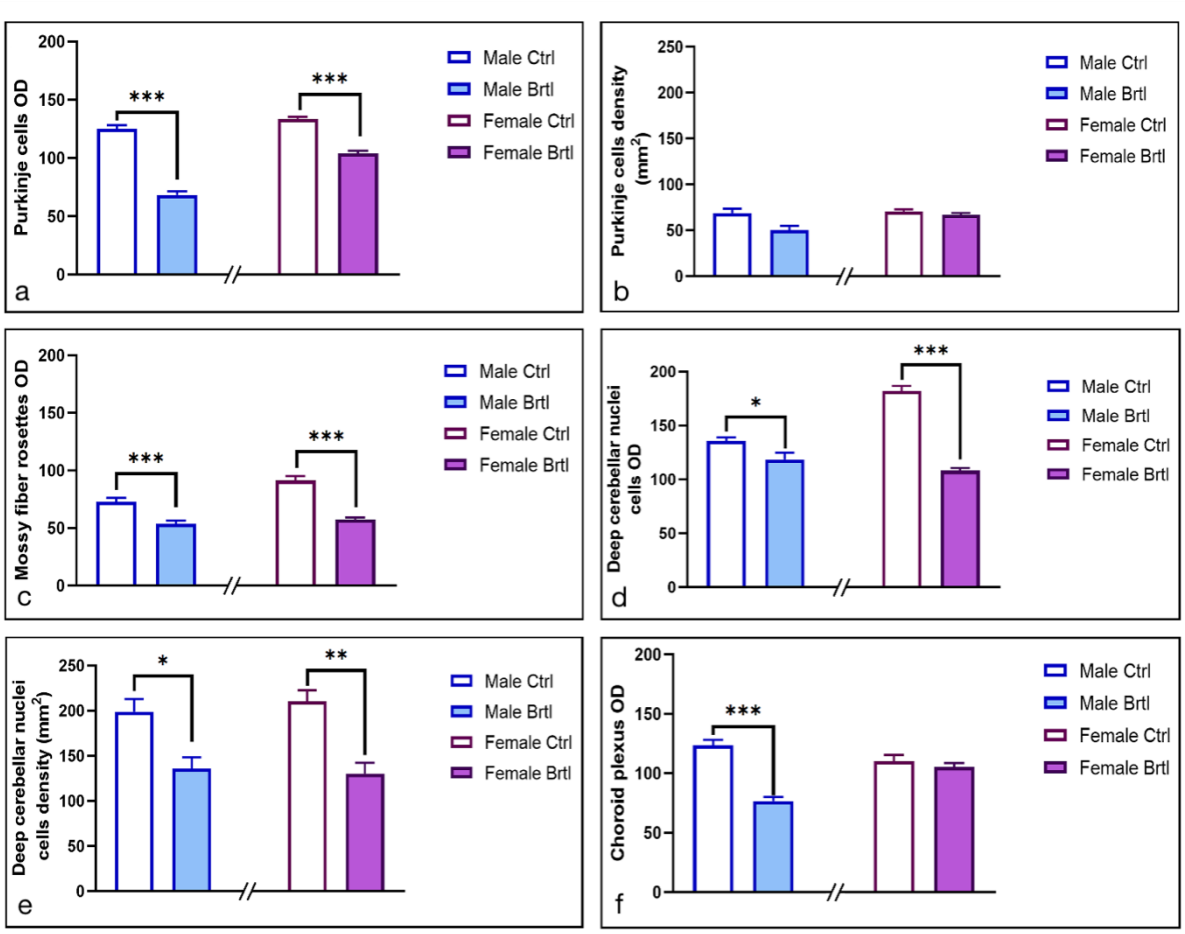

Figure 25. Histograms showing COX4 immunopositive OD and cell density in PCs (a and b), IGL mossy fibers rosettes (c), deep cerebellar nuclei (d and e), and COX4 immunopositive OD in the choroid plexus (f), in male and female mice of the control and Brtl groups. p values: * $p < 0.05$; ** $p < 0.01$; *** $p < 0.001$.

Table 7. Statistical analysis for the quantitative valuation of COX4-immunopositive OD and cell density (n/mm^2) measurements in PC, mossy fibers rosettes, deep cerebellar nuclei and choroid plexus. (ns) not significant; (*) p<0.05; (**) p<0.01; (***) p<0.001.

	Experimental group		**Experimental group**	***p*-value**
OD measurements in PC	Male Ctrl (125.28 ± 3.00)	*vs*	Male Brtl (68.36 ± 3.18)	***
	Female Ctrl (133.65 ± 2.00)	*vs*	Female Brtl (104.13 ± 2.13)	***
PC density (n/mm^2)	Male Ctrl (68.85 ± 4.74)	*vs*	Male Brtl (50.24 ± 4.74)	*ns*
	Female Ctrl (70.71 ± 2.28)	*vs*	Female Brtl (66.99 ± 1.86)	*ns*
OD measurements in mossy fiber rosettes	Male Ctrl (72.84 ± 3.41)	*vs*	Male Brtl (53.62 ± 2.96)	***
	Female Ctrl (91.34 ± 3.99)	*vs*	Female Brtl (57.45 ± 1.75)	***
OD measurements in deep cerebellar nuclei cells	Male Ctrl (38.64 ± 4.43)	*vs*	Male Brtl (29.42 ± 5.59)	*ns*
	Female Ctrl (35.73 ± 5.46)	*vs*	Female Brtl (18.72 ± 2.38)	**
Deep cerebellar nuclei cells density (n/mm^2)	Male Ctrl (199.10 ± 13.99)	*vs*	Male Brtl (135.84 ± 12.69)	*
	Female Ctrl (210.27 ± 12.34)	*vs*	Female Brtl (130.25 ± 12.13)	**
OD measurements in choroid plexus	Male Ctrl (123.67 ± 4.64)	*vs*	Male Brtl (76.71 ± 3.35)	***
	Female Ctrl (110.29 ± 5.25)	*vs*	Female Brtl (105.42 ± 3.40)	*ns*

SOD2 is a critical antioxidant enzyme, located in the mitochondrial matrix, involved in the metabolism of superoxide anion and representing one of the first defense lines against oxidative stress. This antioxidant enzyme is usually used as a specific marker of oxidative stress since SOD2 expression levels are increased in conditions of oxidative damage to counteract ROS elevation (Ishihara et al., 2015; Fu et al., 2016). **Figure 26** reports the results obtained after SOD2 immunostaining. The immunolabelling was mainly localized at the level of PCs and in

the deep cerebellar nuclei of the Brtl cerebellar specimens. Notably, the quantitative analyses reported a highly significant increase in SOD2 immunopositive Purkinje cell OD (**Figure 27, Panel a**) and SOD2 immunopositive deep cerebellar nuclei cell OD (**Figure 27, Panel c**) of both male and female Brtl mice compared to control animals. Similarly, extremely significant is also the increase in immunopositive cells observed in the same cerebellar locations of the pathological mice (**Figure 27, Panel b** and Panel **d**, for PCs and deep cerebellar nuclei cell density, respectively). Contrarily, no significant increase in optical density was detected in the choroid plexus of male or female Brtl specimens, compared to control (**Figure 27, Panel e**) (**Table 8**).

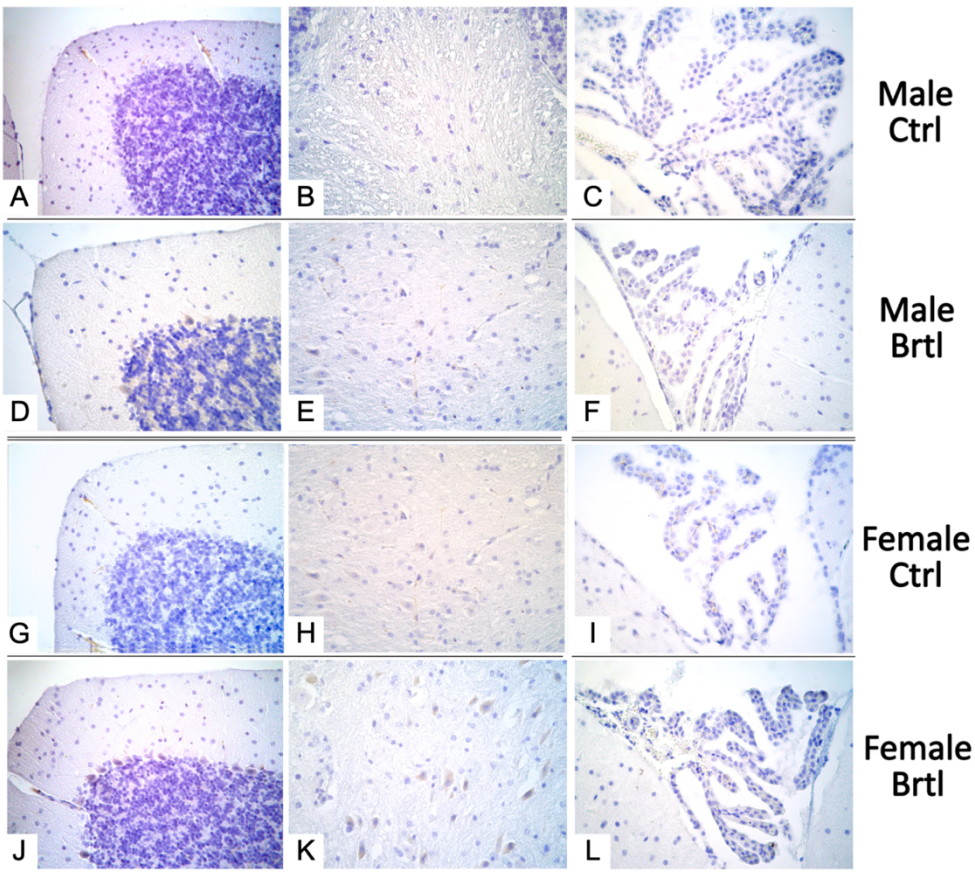

Figure 26. Representative results showing SOD2 immunostaining in cerebellar cortex (A, D, G, and J), deep cerebellar nuclei male (B, E, H, and K), and choroid plexus (C, F, I, and L) in control (A-C and G-I) and Brtl (D-F and J-L) cerebellar slices from male (A-F) and female (G-L) mice. Light microscopy magnification: 40×.

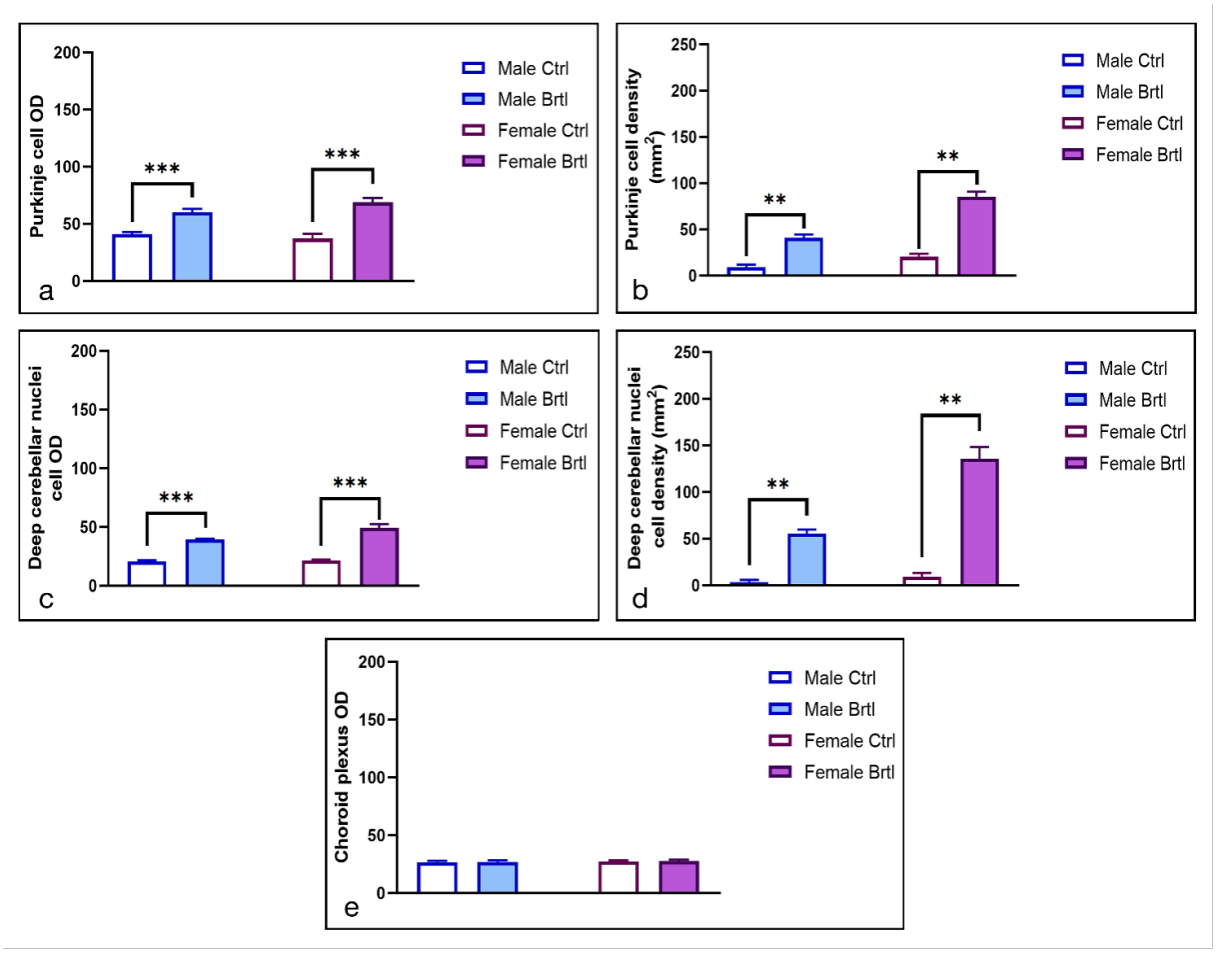

Figure 27. Histograms showing SOD2 immunopositive OD and cell density in PCs (a and b, respectively), deep cerebellar nuclei (c and d, respectively), and SDO2 immunopositive OD in the choroid plexus (e), in male and female mice of the control and Brtl groups. p values: * $p < 0.05$; ** $p < 0.01$; *** $p < 0.001$.

Table 8. Statistical analysis for the quantitative valuation of SOD2-immunopositive OD and cell density (n/mm^2) measurements in PC, mossy fibers rosettes, deep cerebellar nuclei and choroid plexus. (ns) not significant; (**) p<0.01; (***) p<0.001.

	Experimental group		**Experimental group**	***p*-value**
OD measurements in PC	Male Ctrl (41.24 ± 1.60)	*vs*	Male Brtl (37.24 ± 4.21)	***
	Female Ctrl (60.19 ± 3.14)	*vs*	Female Brtl (68.89 ± 3.84)	***
PC density (n/mm^2)	Male Ctrl (9.30 ± 2.94)	*vs*	Male Brtl (40.94 ± 3.72)	**
	Female Ctrl (20.47 ± 3.48)	*vs*	Female Brtl (85.60 ± 5.43)	**
OD measurements in deep cerebellar nuclei	Male Ctrl (20.69 ± 1.08)	*vs*	Male Brtl (39.36 ± 0.84)	***
	Female Ctrl (21.73 ± 0.74)	*vs*	Female Brtl (49.51 ± 3.04)	***
Deep cerebellar nuclei cells density (n/mm^2)	Male Ctrl (3.72 ± 2.28)	*vs*	Male Brtl (55.82 ± 4.16)	**
	Female Ctrl (9.30 ± 4.16)	*vs*	Female Brtl (135.84 ± 12.69)	**
OD measurements in choroid plexus	Male Ctrl (26.72 ± 1.39)	*vs*	Male Brtl (27.08 ± 1.39)	*ns*
	Female Ctrl (27.35 ± 0.99)	*vs*	Female Brtl (27.92 ± 1.10)	*ns*

GPx4, a member of the selenium-containing GPx family, is another key antioxidant enzyme responsible for the reduction of phospholipid peroxides into the correspondent alcohols; thereby GPx4 participates in the detoxification of membrane lipid peroxides and plays a critical role in controlling cell homeostasis, while decreased activity in this enzyme is associated with increased levels of oxidative stress (Pei et al., 2023). **Figure 28** shows the most representative micrographs highlighting GPx4 immunostaining results: under control conditions, GPx4 signal is well detectable in both the cytoplasmatic and nuclear compartments of the cells. Conversely, a decrease in GPx4 staining was observed in the pathological condition. As reported in the histograms shown in **Figure 29**, an extremely significant reduction in GPx4 OD and cell density

is observed in PCs (**Figure 29, Panel a** and **Panel b**, for GPx4 immunopositive OD and cell density, respectively) and in the deep cerebellar nuclei (**Figure 29, Panel c** and **Panle d**, for GPx4 immunopositive OD and cell density, respectively) of male and female Brtl mice, compared to control animals. Similarly, an extremely significant decrease in GPx4 positivity is detected in the choroid plexus (**Figure 29, Panel e**) of Brtl specimens, both in male and female mice. It should be noted that a significant reduction was also observed in the density of immunopositive cells in the deep cerebellar nuclei, as well as in the density of immunopositive Purkinje cells in both male and female Brtl mice (**Table 9**).

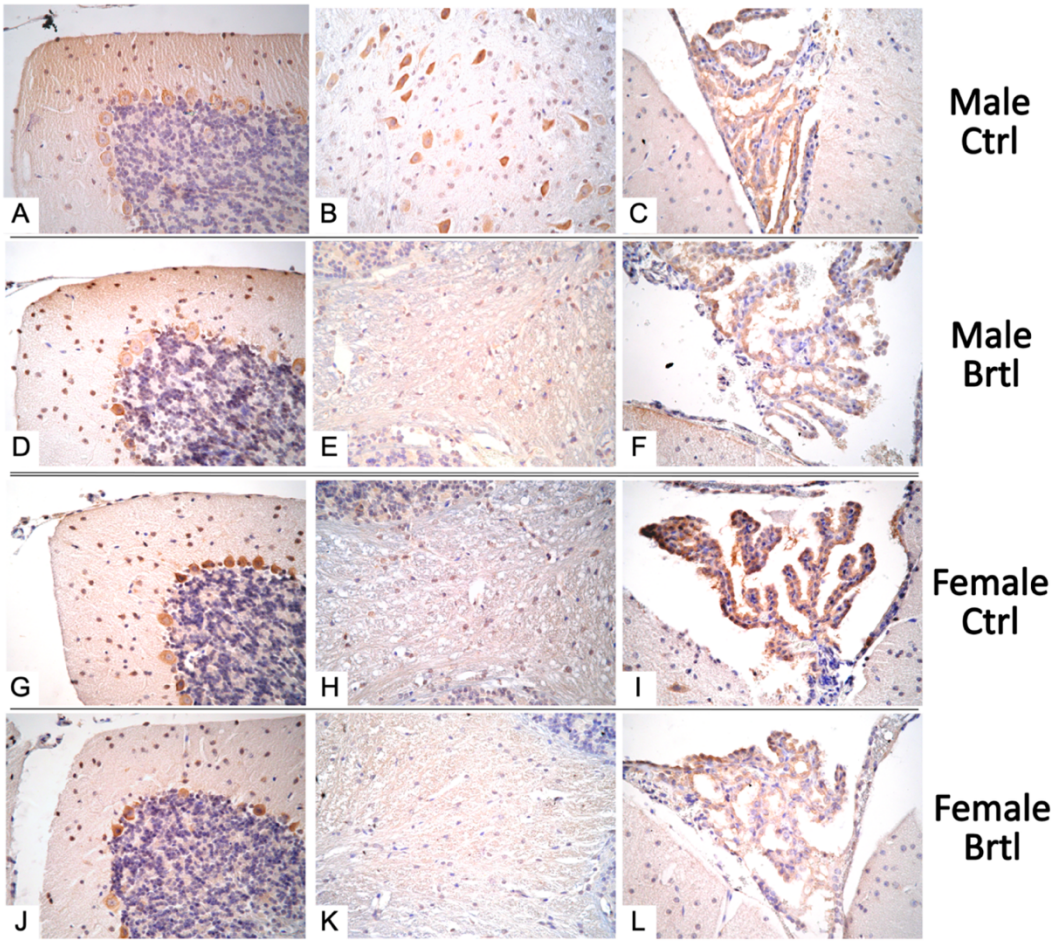

Figure 28. Representative results showing GPx4 immunostaining in cerebellar cortex (A, D, G, and J), deep cerebellar nuclei (B, E, H, and K), and choroid plexus (C, F, I, and L) of control (A-C and G-I) and Brtl (D-F and J-L) cerebellar slices in male (A-F) and female (G-L) mice. Light microscopy magnification: 40×.

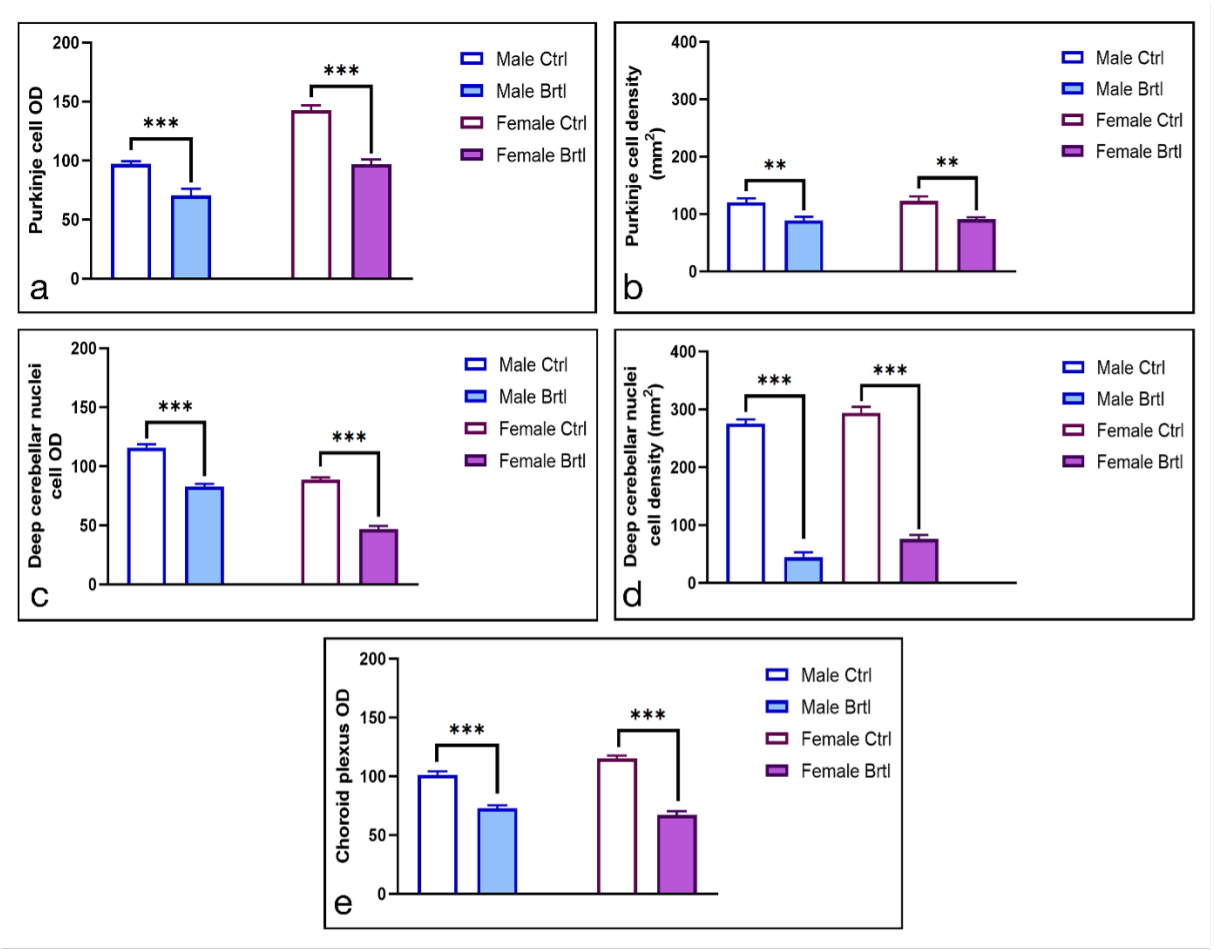

Figure 29. Histograms showing GPx4 immunopositive OD and cell density in PCs (a and b respectively), deep cerebellar nuclei (c and d respectively), and GPx4 immunopositive OD in the choroid plexus (e), in male and female mice of the control and Brtl groups. p values: ** $p < 0.01$; *** $p < 0.001$.

Table 9. Statistical analysis for the quantitative valuation of GPx4-immunopositive OD and cell density (n/mm^2) measurements in PC, mossy fibers rosettes, deep cerebellar nuclei and choroid plexus. (**) p<0.01; (***) p<0.001.

	Experimental group		**Experimental group**	***p*-value**
OD measurements in PC	Male Ctrl (97.18 ± 2.35)	*vs*	Male Brtl (70.64 ± 5.67)	***
	Female Ctrl (142.74 ± 4.10)	*vs*	Female Brtl (97.01 ± 4.12)	***
PC density (n/mm^2)	Male Ctrl (120.95 ± 6.58)	*vs*	Male Brtl (89.32 ± 6.31)	**
	Female Ctrl (122.81 ± 8.00)	*vs*	Female Brtl (91.18 ± 3.48)	**
OD measurements in deep cerebellar nuclei	Male Ctrl (115.98 ± 2.82)	*vs*	Male Brtl (82.79 ± 2.38)	***
	Female Ctrl (88.77 ± 1.81)	*vs*	Female Brtl (47.07 ± 2.54)	***
Deep cerebellar nuclei cells density (n/mm^2)	Male Ctrl (275.40 ± 7.56)	*vs*	Male Brtl (44.66 ± 8.53)	***
	Female Ctrl (294.00 ± 10.44)	*vs*	Female Brtl (76.29 ± 6.84)	***
OD measurements in choroid plexus	Male Ctrl (101.30 ± 3.00)	*vs*	Male Brtl (72.80 ± 2.54)	***
	Female Ctrl (115.34 ± 2.38)	*vs*	Female Brtl (67.25 ± 3.13)	***

NRF2 is a transcription factor that plays an extensive role in regulating several signaling pathways related to macromolecules and iron metabolism, oxidative stress, and serves as a key regulator of the antioxidant systems. In 56hysiologicalcal conditions, NRF2 remains confined to the cytoplasm where it is targeted for ubiquitin-mediated degradation. However, in case of redox imbalance, this transcription factor moves to the nucleus where it activates the transcription of genes coding for numerous antioxidant enzymes (Dodson et al., 2019). Different NRF2 expression levels are displayed in the cerebellum of control and pathological Brtl mice (**Figure 30**), with a more evident immunopositivity detected in the cerebellum of pathological animals. In particular, the results of the quantitative analyses shown in **Figure 31**

confirm a highly significant increase in NRF2 immunopositive OD of male and female Brtl in PCs (**Figure 31, Panel a**) and deep cerebellar nuclei (**Figure 31, Panel c**), compared to control groups. In addition, the cortical area shows an extremely significant increase of immunopositive PCs density (**Figure 31, Panel b**) in Brtl mice of both genders. Similarly, NFR2 immunopositive cell density is also significantly increased in the cells of deep cerebellar nuclei (**Figure 31, Panel d**) of mutated groups, compared to control. Parallelly, the choroid plexus (**Figure 31, Panel e**), of male Brtl mice displayed only a significant increase of NRF2 OD; conversely, in female Brtl animals an extremely significant increase was observed (**Table 10**).

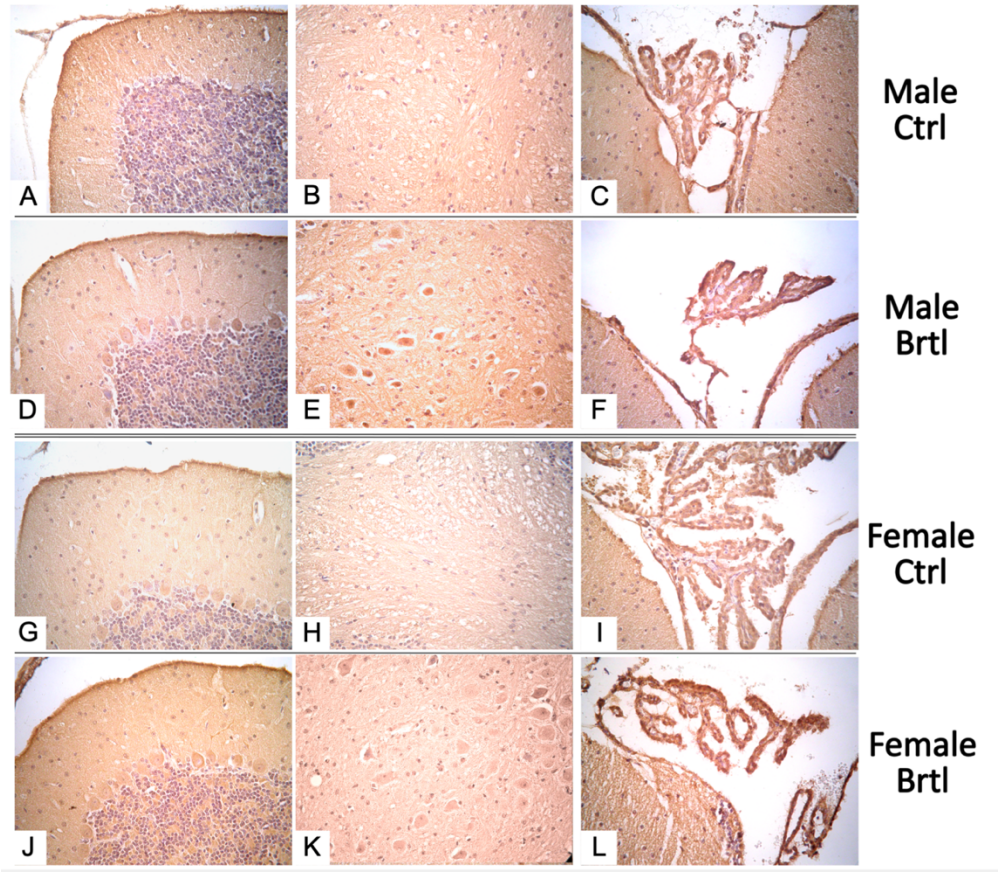

Figure 30. Representative results showing NRF2 immunostaining in cerebellar cortex (A, D, G, and J), deep cerebellar nuclei (B, E, H, and K), and choroid plexus (C, F, I, and L) of control (A-C and G-I) and Brtl (D-F and J-L) cerebellar slices in male (A-F) and female (G-L) mice. Light microscopy magnification: 40×.

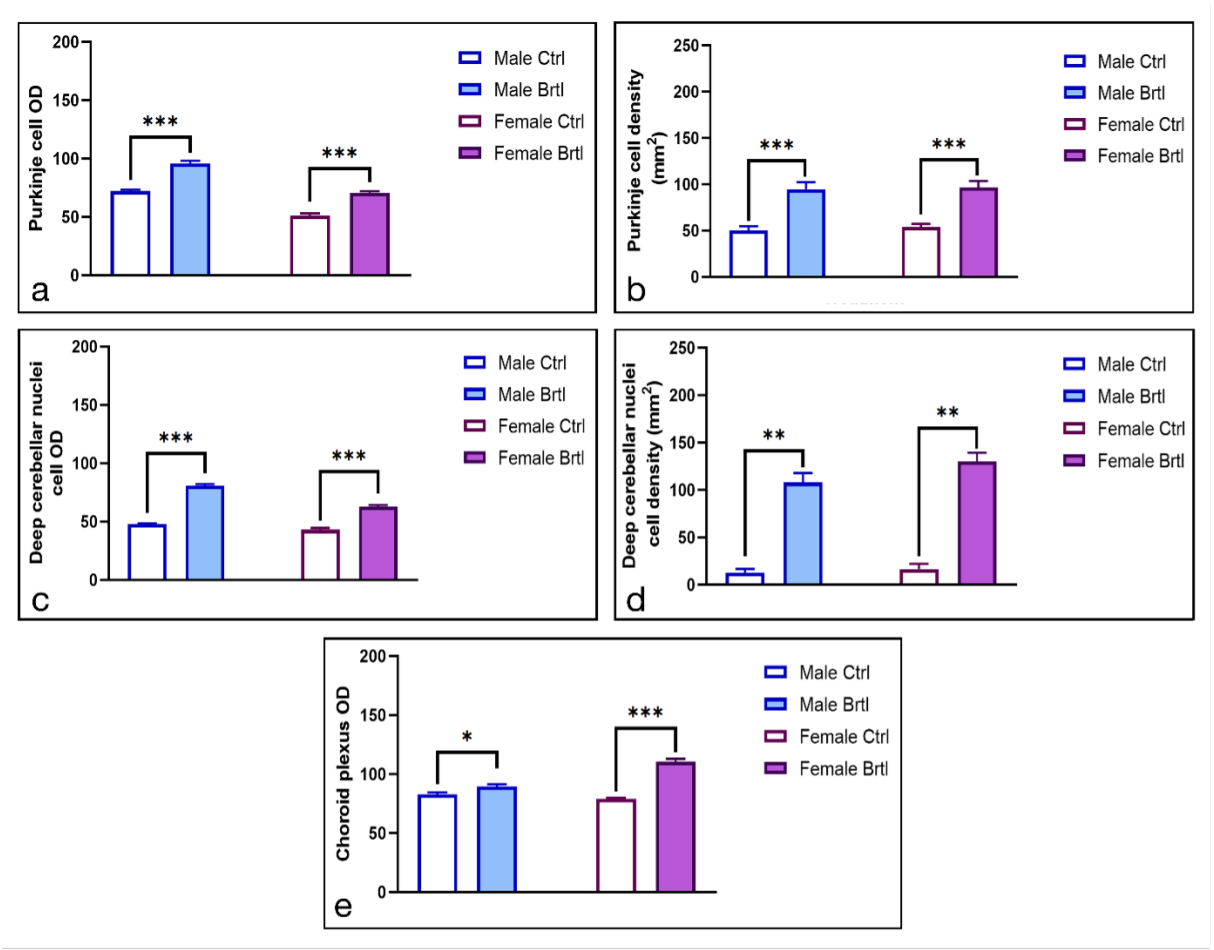

Figure 31. Histograms showing NRF2 immunopositive OD and cell density in PCs (a and b respectively), deep cerebellar nuclei (c and d respectively), and NRF2 immunopositive OD in the choroid plexus (e), in male and female mice of the control and Brtl groups. p values: * $p < 0.5$; ** $p < 0.01$; *** $p < 0.001$.

Table 10. Statistical analysis for the quantitative valuation of NRF2-immunopositive OD and cell density (n/mm^2) measurements in PC, mossy fibers rosettes, deep cerebellar nuclei and choroid plexus. (*) p<0.5; (**) p<0.01; (***) p<0.001.

	Experimental group		Experimental group	p-value
OD measurements in PC	Male Ctrl (72.26 ± 1.39)	*vs*	Male Brtl (95.73 ± 2.46)	***
	Female Ctrl (51.18 ± 1.97)	*vs*	Female Brtl (70.67 ± 1.46)	***
PC density (n/mm^2)	Male Ctrl (50.24 ± 4.74)	*vs*	Male Brtl (94.90 ± 7.44)	***
	Female Ctrl (53.96 ± 3.48)	*vs*	Female Brtl (96.76 ± 6.96)	***
OD measurements in deep cerebellar nuclei	Male Ctrl (47.73 ± 0.91)	*vs*	Male Brtl (80.82 ± 1.51)	***
	Female Ctrl (43.10 ± 1.69)	*vs*	Female Brtl (62.97 ± 1.53)	***
Deep cerebellar nuclei cells density (n/mm^2)	Male Ctrl (13.03 ± 3.72)	*vs*	Male Brtl (107.93 ± 10.02)	**
	Female Ctrl (16.75 ± 5.43)	*vs*	Female Brtl (130.26 ± 9.30)	**
OD measurements in choroid plexus	Male Ctrl (82.73 ± 1.93)	*vs*	Male Brtl (89.49 ± 1.87)	*
	Female Ctrl (79.02 ± 1.08)	*vs*	Female Brtl (110.55 ± 2.56)	***

5. Discussion

Despite being a genetically and phenotypically heterogeneous disease, the unifying feature of Osteogenesis Imperfecta is the collagen-related defects that result from mutations in numerous genes involved in collagen synthesis, folding, and processing; all the different mutations associated with the disease pathophysiology ultimately lead to qualitative and quantitative alterations in collagen, responsible for the most well-known clinical features observed in OI patients: bone fragility, susceptibility to fractures, and growth deficiency. Approximately 85% of cases report defects in collagen type I structure or quantity, due to mutations in the genes encoding for the α1 and α2 chains of type I procollagen (*Col1A1* and *Col1A2*, respectively) (Yu et al., 2023). Collagen type I is the most abundant fibrous protein of the extracellular matrix, which offers structural and biochemical support to the surrounding cells: the ECM grants mechanical resistance and regulates crucial cellular functions such as cell adhesion and communication (Amirrah et al., 2022). Specifically, in the central nervous system, the ECM also holds active roles fundamental for neuronal and glial cell growth and functionality: it modulates homeostasis by regulating the ionic environment, provides neuronal protection by forming barriers and supporting tissue repair after injuries, regulates and influences synaptic functions by influencing neurotransmitter release or receptor availability (Wareham et al., 2024). Moreover, in the nervous system, the extracellular matrix plays a critical role during cell migration. In fact, during neural development, ECM components guide neurons toward their final localization, facilitating the proper formation of neuronal networks (Long & Huttner, 2019). Therefore, the ECM and its constituents not only offer passive structural support but also influence the ability to respond to stress, ensuring stability within the neuronal and vascular components in the CNS and defects in collagen type I result in alterations of the interplay between ECM, neurons, and glial cells (Wareham et al., 2024). Literature has evidenced the complex crosstalk between ECM remodeling and DNA damage/oxidative stress. The interactions between these two elements are bidirectional: DNA damage and an increase in ROS content can negatively affect ECM homeostasis; nonetheless, mutations in ECM genes strongly affect tissue and cell homeostasis, by triggering the accumulation of ROS, thereby causing an increase in reactive oxygen species (Martins et al., 2021). Collagen synthesis and stability are modulated by oxidative stress and previous literature data highlighted that collagen deficiency correlates with increased oxidative stress, elevating ROS production and contributing to mitochondrial dysfunctions. On the other hand, increased levels of oxidative

stress, in the presence of collagen type I deficiency, has been suggested to exacerbate OI bone symptomatology (Long & Huttner, 2019).

Based on this issue, the proposed thesis work evaluated the morphological alterations and analyzed the expression levels of collagen as well as specific oxidative stress markers (COX4, SOD2, GPX4, and NRF2) in the CNS of Brtl OI mouse model, bearing the G349C substitution in the *Col1A1* allele. Specifically, this study focalized their attention on the cerebellum, a region of the CNS crucial for coordination, balance, motor learning and other cognitive functions. The evaluations, conducted using bright field and polarized light microscopy, evidenced the presence of profounds morphological and cytoarchitectural differences in the cerebellar tissue of mutant animals: substantial cytoarchitectural defects are shown in the cerebellar specimens of Brtl mice, denoted by a significant reduction in cell density in both the molecular and granule layer of the cerebellum. The cause of this strong morphological modification could be attributed to the abnormal development of the cerebellar cortex during the early postnatal phases, probably linked to the improper migration of granule cells from the external granule layer to the internal granule layer, that takes place during the first few weeks of postnatal NS development in mice, and the subsequent arising of migratory defects of several cell type during the formation of the molecular layer (Komuro et al., 2013). In this regard, previous studies highlighted the role played by ECM constituents, specifically by collagens and laminins, in the differentiative and migratory processes occurring in the CNS. Particularly, during the development of the cerebellum, ECM components are transiently expressed, in specific locations, and interact with target surface receptors . Microarray analyses highlighted that several collagen types (including collagen type I) are expressed with a tight spatiotemporal pattern during cerebellar development, i.e. higher levels of collagen are observed early on, while later they decrease (Hatten et al., 1982; Wéber et al., 2024). Notably, as development progresses, collagen expression remains spatially associated with the PC layer. Additionally, the correlated co-expression individuated between collagens and other ECM components implies a potential synergistic, functional role played by the ECM proteins during the development of the cerebellum and, specifically, of the survival and differentiation of PCs (Duband & Thiery, 1987).

Our study clearly detected a significant reduction of collagen expression levels in both male and female Brtl mice. These changes in collagen levels affected the more superficial cerebellar meninges as well as the deeper structures, such as the choroid plexus. Specifically, the

observations conducted using PSR staining under polarized light microscopy revealed that this reduction primarily influenced mature collagen fibers while the levels of immature fibers were less impacted in male mice. These findings on the one hand likely suggest an impairment concerning collagen maturation processes. Moreover, the gender difference in the collagen expression levels detected in our study suggests a possible dissimilarity in the susceptibility to collagen depletion.

ECM components, including collagen type I, are critical constituents of the meningeal layers; in particular, collagen type I is highly expressed by several cell types in the brain, including meningeal cells (Wareham et al., 2024). Remarkably, the meninges not only contribute to the brain's protection and support but also play crucial roles in CNS vascularisation and neural development (Siegenthaler & Pleasure, 2011). Accordingly, the alterations in the levels of mature collagen reported in the meninges of mutant animals validate the hypothesis that there may be defects in neuronal migration, and these in turn may subtend the morphological alterations of the cerebellar cortex.

Furthermore, current research regarding the expression of collagens in the choroid plexus of aged and injured brains evidenced immunoreactivity for collagen type I in the stroma, below the choroidal epithelial cells (Wakamatsu et al., 2022). The choroid plexus consists of a layer of epithelial cells, lined by meningeal cells, and a network of capillaries; this vital structure plays critical role in the CNS, producing the cerebrospinal fluid (CSF), which maintains brain homeostasis and conveys immunological signals, and representing the blood-CSF barrier, separating and protecting the brain from the periphery (Javed et al., 2024). Additionally, the choroid plexus also produces and releases growth factors and parallelly maintains the subventricular zone stem cell pool (Falcão et al., 2012). Therefore, abnormalities in the choroid plexus are associated with a broad range of neurological conditions: hydrocephalus, encephalopathies, and neurometabolic diseases have been associated with morphological alterations of the choroid plexus (Kaur et al., 2016); moreover, changes in choroid plexus morphology which could lead to the loss of choroid plexus secretory may contribute to the progression of neurodegenerative diseases, including Alzheimer's Disease and Multiple Sclerosis (Kratzer et al., 2020). Collagen type I is expressed in the choroid plexus, and alterations in collagen expression may contribute to choroid plexus alterations observed in aged brains (Tahira et al., 2021). Therefore, a reduction in collagen expression levels or its incomplete/altered maturation in the choroid plexus, as reported in the present study, may lead

to morphological and functional abnormalities in this critical CNS structure; this may result in the loss of its ability to form a neuroprotective barrier for the brain and to secrete and control the composition of CSF, which in turn influences the behaviour of stem cells lining the ventricles, thereby impairing the regulation of neurogenesis (Johansson, 2014).

Evaluations of the redox balance revealed a substantial alteration in the oxidative stress pathway, both in superficial and deeper cerebellar regions, and a differential susceptibility between genders in specific areas. The COX4 is a component of the cytochrome c oxidase (COX) enzyme complex, or complex IV, working as the terminal electron acceptor during mitochondrial oxidative phosphorylation (Sinkler et al., 2017). COX4 participates in the assembly and functioning of COX, by inhibitory feedback of COX activity in the presence of high ATP concentrations (Bikas et al., 2020). COX4 is present in two isoforms: (i) COX4-1 is ubiquitously expressed in mammalians under physiological conditions while (ii) COX4-2, normally less expressed than COX4-1, is upregulated under oxidative stress conditions since it is suggested to enhance COX enzyme activity (Douiev et al., 2021). The present study evidenced that in the cerebellar cortex, COX4 immunostaining was overall lower in both male and female Brtl mice compared to the controls, while the deep cerebellar nuclei and the choroid plexus showed a different pattern of expression in the two sexes. In particular, the deep cerebellar nuclei in female animals exhibited a more evident reduction in COX4 staining, differently, in males a more marked decrease in COX4 expression was evidenced in the choroid plexus. A decrease in COX4 expression observed in our data may indicate increased oxidative stress and therefore subtend overall mitochondrial perturbations, which can in turn trigger further ROS increase. In the CNS, this increase in ROS levels could translate into altered synaptic transport and functionality, which finally result in neural plasticity impairments (Kriebel et al., 2020).

Superoxide dismutase 2 (SOD2), located in the mitochondrial matrix, is one of the main cellular detoxifying enzymes; SOD2 catalyzes the dismutation of the superoxide anion, a reactive radical, into hydrogen peroxide and acts as a fundamental antioxidant agent against the oxidative damage produced by mitochondria during oxidative phosphorylation (Palma et al., 2020). In this regard, our results clearly demonstrated a significant increase in SOD2 expression across the whole cerebellar cortex and in the deep cerebellar nuclei of mutant OI mice, potentially suggesting an attempt of cells to counteract the redox imbalance observed in these animals via SOD2 upregulation. Through specific molecular pathways, excessive ROS

concentrations can activate SOD2 expression and increase its activity, which in turn modulates cellular antioxidant responses by reducing ROS production, thereby protecting mitochondria and to ensure cell survival in conditions of oxidative damage (Kim et al., 2017; Zuo et al., 2019). Additionally, our data evidenced a gender-specific increase in SOD2 expression levels, which appear higher in female Brtl mice than in males of the same group; these results may indicate either a more prominent production of ROS or a more efficient antioxidant system in female mutants.

Among the numerous antioxidant defenses available to cells, there is GPx4, an antioxidant enzyme that modulates oxidative stress levels by reducing lipid peroxides to alcohols while simultaneously oxidizing glutathione to glutathione disulfide. GPx4 plays a fundamental role in managing oxidative stress and ferroptosis, a form of programmed cell death, because it inhibits the interaction of peroxides with redox-active ferrous ions, which would otherwise lead to the propagation of reactive oxygen species (ROS) (Jiang et al., 2021). However, prolonged mitochondrial dysfunctionality and chronic redox imbalance can change physiological GPx4 processing. In particular, fumarate accumulation, due to altered mitochondrial functionality, irreversibly modifies GPx4, compromising its functionality and propagating oxidative damage (Cui et al., 2022). Moreover, GPx4 has been proven essential in maintaining homeostasis both during development and in neurons of adult mice, where it improves neuronal health and survival (Chen et al., 2015; Wei, 2024). Consequently, the significant reduction in GPx4 expression levels observed in the cerebellar cortex and deep nuclei of male and female Brtl mice may subtend an increased risk of lipid peroxides accumulation which may in turn lead to a possible ferroptosis cell death activation. Ferroptosis is involved in the progression of numerous pathologies, including nervous system and neurologic disease (Ou et al., 2022). Indeed, acute nervous system injuries such as inschemic stroke and traumatic brain injury both involve ferroptosis as primary mechanism of cell-death, linked to GPx4 depletion or dysfunctionality (Wenzel et al., 2017; Chen et al., 2021). Moreover, ferroptosis and abnormal iron dynamics have been suggested to be tightly linked to the pathophysiology of neurodegenerative diseases, including Alzheimer's Disease and Amiotrofic Lateral Sclerosis, where it mediates neuronal oxidative damage and, subsequently, neuronal death (Ou et al., 2022). Consistently, studies have evidenced that GPx4-deficient adult mice showed substantial neuronal loss in the CNS (Yoo et al., 2012).

An additional cellular defense mechanism against reactive oxygen species is represented by NRF2, a key transcription factor activated by inflammation and oxidative damage, which acts by upregulating the expression levels of specific antioxidant genes (Dodson et al., 2019). In the CNS, NRF2 is expressed by glial cells and neurons in response to oxidative damage (Heurtaux et al., 2022). Under physiological conditions, cytoplasmatic NRF2 is bound to Kelch-like ECH-associated protein 1 (KEAP1), a negative regulator that drives NRF2 degradation. Conversely, the accumulation of ROS causes the oxidation of cysteine residues on KEAP1, altering its structure and leading to the release of NRF2 (Baird & Yamamoto, 2020). In this stressed condition, NRF2 is phosphorylated and translocates to the nucleus, where it drives the expression of target genes such as antioxidant enzymes and components of the mitochondrial respiratory complex (Baird & Yamamoto, 2020; Dinkova-Kostova & Abramov, 2015). Therefore, the increased levels of cytoplasmic NRF2 in the cerebellum of Brtl mice observed in our study may suggest the activation of stress-induced mechanisms that, through the blockade of NRF2 negative regulator system by ROS accumulation, lead to cytoplasmatic accumulation of NRF2 that aims at boosting the transcription of antioxidant genes to fight oxidative stress damage. However, current literature reports that ageing and persistent stress can severely impact the normal functionality of the NRF2 pathway; consequently, the impaired ability to respond to increased ROS influences all of those elements that are targeted by NRF2 (Díaz et al., 2024).

6. Conclusions and Future Perspectives

Osteogensis imperfecta (OI) is a rare, genetic collagen-related disorder affecting approximately 1 in every 10.000-20.000 newborns. It is a highly heterogeneous condition, both genetically and phenotypically, with a broad range of symptomatologies: bone fragility, susceptibility to fractures and skeletal deformities, as well as a wide array of serious secondary manifestations (Rapoport et al., 2023). Particularly, the pathology also has implications on the nervous system: OI patients report craniocervical abnormalities, such as cerebellar displacement and hypoplasia, and alterations in the cerebrovascular system (Husain et al., 2024; Emery et al., 1999). Moreover, the brain parenchyma can be affected, and neuropathological findings have evidenced defects in neuronal migration and differentiation (Khandanpour et al., 2012; Emery et al., 1999). In some cases, children affected by OI exhibit marked neurodevelopmental delays, involving motor skills and speech (Efthymiou et al., 2021). Therefore, the disease poses severe challenges in the life of OI patients and can severely impact their daily activities and the overall quality of life (Hill et al., 2022).

The present study evidenced morphological alterations and an increase in oxidative stress within different cell populations and cerebellar regions of the Brtl murine model. These data might indicate a connection between motor learning deficits, as well as balance and coordination impairments observed in OI patients with the damages to the CNS caused by the increased oxidative stress levels and, potentially, by the activation of specific cell death mechanisms, deriving altogether from the defects in collagen type I.

To date, it is still unclear whether the increase in oxidative stress levels is driven by an increase in inflammation or vice versa. Therefore, further studies could aim to investigate the inflammatory pathways in this murine model of OI more accurately, seeking to clarify which mechanism is activated first in the CNS of these mutated animals. Moreover, further research focused on oxidative stress pathway could provide better insights into the regulation of these mechanisms in OI pathology, possibly investigating the expression levels of specific molecules directly involved in the defensive mechanisms against ROS overproduction, e.g. KEAP1, which could enable better dissection of the KEAP1-NRF2 pathway and further understand the significance of NRF2 cytoplasmic increase as well as potentially unveil other players involved in the translocation of this transcription factor into the nucleus. Further investigations could simultaneously shed light on the involvement of different programmed cell death mechanisms

activated in this pathological condition by exploring the potential activation of apoptotic, autophagic, or necroptotic pathways. This could provide a comprehensive understanding of the possible interactions between oxidative stress, inflammation, and cell death pathways in the CNS of the OI murine model. Equally important would be to study the possible morphological and cellular alterations resulting from the presence of this mutated collagen isoform, as well as the activation of the aforementioned oxidative stress, inflammation, and cell death pathways in other areas of the nervous system involved in motor control, such as the motor cortex.

In conclusion, this thesis work provides a new perspective and opens new insights into the almost unexplored relationship between the CNS and OI, paving the way for further research to improve OI management and the overall quality of life of OI patients. Further studies are to be conducted to investigate in greater detail the cognitive implications of mutant collagen type I in the cerebellum, potentially through the implementation of behavioral studies on *in vivo* models and with clinical trials.

Bibliography

Alcorta-Sevillano N. et al. Murine Animal Models in Osteogenesis Imperfecta: The Quest for Improving the Quality of Life. Int. J. Mol. Sci. 2022; 24: 184.

Amirrah I.N. et al. A Comprehensive Review on Collagen Type I Development of Biomaterials for Tissue Engineering: From Biosynthesis to Bioscaffold. Biomedicines. 2022; 10: 2307.

Arponen H. et al. Fatigue and disturbances of sleep in patients with osteogenesis imperfecta – a cross-sectional questionnaire study. BMC Musculoskelet. Disord. 2018; 19: 3

Baird L. & Yamamoto M. The Molecular Mechanisms Regulating the KEAP1-NRF2 Pathway. Mol. Cell. Biol. 2020; 40: e00099-20.

Beh S.C. et al. M. Cerebellar Control of Eye Movements. J. Neuroophthalmol. 2017; 37: 87.

Bianchi L. et al. Differential response to intracellular stress in the skin from osteogenesis imperfecta Brtl mice with lethal and non lethal phenotype: A proteomic approach. J. Proteomics. 2012; 75: 4717–4733.

Bikas A. et al. Cytochrome C Oxidase Subunit 4 (COX4): A Potential Therapeutic Target for the Treatment of Medullary Thyroid Cancer. Cancers. 2020; 12: 2548.

Bini L. et al. Intracellular and Extracellular Markers of Lethality in Osteogenesis Imperfecta: A Quantitative Proteomic Approach. Int. J. Mol. Sci. 2021; 22: 429.

Blouin S. et al. Cortical bone properties in the Brtl/+ mouse model of Osteogenesis imperfecta as evidenced by acoustic transmission microscopy. J. Mech. Behav. Biomed. Mater. 2019; 90: 125–132.

Bourens M. ete al. Redox and Reactive Oxygen Species Regulation of Mitochondrial Cytochrome c Oxidase Biogenesis. Antioxid. Redox Signal. 2013; 19: 1940–1952.

Buffo A. & Rossi F. Origin, lineage and function of cerebellar glia. Prog. Neurobiol. 2013; 109: 42–63

Butler A.B. & Hodos W. Comparative vertebrate neuroanatomy: evolution and adaptation. Wiley-Interscience, Hoboken. 2005.

Carulli D. et al. Cerebellar plasticity and associative memories are controlled by perineuronal nets. Proc. Natl. Acad. Sci. 2020; 117: 6855–6865.

Cerrato V. Cerebellar Astrocytes: Much More Than Passive Bystanders In Ataxia Pathophysiology. J. Clin. Med. 2020; 9: 757.

Chen J. et al. Inhibition of Acyl-CoA Synthetase Long-Chain Family Member 4 Facilitates Neurological Recovery After Stroke by Regulation Ferroptosis. Front. Cell. Neurosci. 2021; 15: 632354.

Chen L. et al. Ablation of the Ferroptosis Inhibitor Glutathione Peroxidase 4 in Neurons Results in Rapid Motor Neuron Degeneration and Paralysis. J. Biol. Chem. 2015; 290: 28097–28106.

Chizhikov V.V. et al. Lmx1a regulates fates and location of cells originating from the cerebellar rhombic lip and telencephalic cortical hem. Proc. Natl. Acad. Sci. U. S. A. 2015; 107: 10725–10730.

Coêlho G. et al. Postural balance, handgrip strength and mobility in Brazilian children and adolescents with osteogenesis imperfecta. J. Pediatr. (Rio J.). 2021; 97: 315–320.

Consalez G.G. et al. Origins, Development, and Compartmentation of the Granule Cells of the Cerebellum. Front. Neural Circuits. 2021; 14: 611841.

Cui C., Yang F. & Li Q. Post-Translational Modification of GPX4 is a Promising Target for Treating Ferroptosis-Related Diseases. Front. Mol. Biosci. 2022; 9: 901565.

De Zeeuw C.I. et al. Recording Eye Movements in Mice: A New Approach to Investigate the Molecular Basis of Cerebellar Control of Motor Learning and Motor Timing. Otolaryngol. Neck Surg. 1998; 119: 193–203.

Díaz M. et al. Age-Dependent Changes in Nrf2/Keap1 and Target Antioxidant Protein Expression Correlate to Lipoxidative Adducts, and Are Modulated by Dietary N-3 LCPUFA in the Hippocampus of Mice. Antioxidants. 2024; 13: 206.

Dinkova-Kostova A.T. & Abramov A.Y. The emerging role of Nrf2 in mitochondrial function. Free Radic. Biol. Med. 2015; 88: 179–188.

Dodson M. et al. NRF2 plays a critical role in mitigating lipid peroxidation and ferroptosis. Redox Biol. 2019; 23: 101107.

Douiev L. et al. Upregulation of COX4-2 via HIF-1α in Mitochondrial COX4-1 Deficiency. Cells. 2021; 10: 452.

Duband J.-L. & Thiery J.P. Distribution of laminin and collagens during avian neural crest development. Development. 1987; 101: 461–478.

Engelbert R.H.H. et al. Osteogenesis imperfecta: profiles of motor development as assessed by a postal questionnaire. Eur. J. Pediatr. 2000; 159: 615–620.

Efthymiou S. et al. Two novel bi-allelic KDELR2 missense variants cause osteogenesis imperfecta with neurodevelopmental features. Am. J. Med. Genet. A. 2021; 185: 2241–2249.

Emery S.C. et al. Abnormalities in Central Nervous System Development in Osteogenesis Imperfecta Type II. Pediatr. Dev. Pathol. 1999; 2: 124–130.

Etich J. et al. Signaling pathways affected by mutations causing osteogenesis imperfecta. Cell. Signal. 2020; 76: 109789.

Falcão A.M. et al. The path from the choroid plexus to the subventricular zone: go with the flow!. Front. Cell. Neurosci. 2012; 6: 34.

Fu Y. et al. Aging Promotes SIRT3-dependent Cartilage SOD2 Acetylation and Osteoarthritis. Arthritis Rheumatol. Hoboken NJ. 2016; 68: 1887–1898.

Fujita H. et al. Modular output circuits of the fastigial nucleus for diverse motor and nonmotor functions of the cerebellar vermis. eLife. 2020; 9: e58613.

Hart T. et al. The IMPACT Survey: the economic impact of osteogenesis imperfecta in adults. Orphanet J. Rare Dis. 2024; 19: 222.

Heurtaux T. et al. Normal and Pathological NRF2 Signalling in the Central Nervous System. Antioxidants. 2022; 11: 1426.

Hill M. et al. Living with osteogenesis imperfecta: A qualitative study exploring experiences and psychosocial impact from the perspective of patients, parents and professionals. Disabil. Health J. 2022; 15: 101168.

Hirono M. et al. Perineuronal Nets in the Deep Cerebellar Nuclei Regulate GABAergic Transmission and Delay Eyeblink Conditioning. J. Neurosci. 2018; 38: 6130–6144.

Hubert T. et al. Collagens in the developing and diseased nervous system. Cell. Mol. Life Sci. CMLS. 2009; 66: 1223–1238.

Husain T.S. et al. Neurocranial growth in the OIM mouse model of osteogenesis imperfecta. Anat. Rec. 2024; 307: 581–591.

Ishihara Y. et al. Dual Role of Superoxide Dismutase 2 Induced in Activated Microglia: OXIDATIVE STRESS TOLERANCE AND CONVERGENCE OF INFLAMMATORY RESPONSES*. J. Biol. Chem. 2015; 290: 22805–22817.

Javed K. et al., Neuroanatomy, Choroid Plexus. StatPearls, StatPearls Publishing, Treasure Island (FL). 2024.

Jiang X. et al. 2021. Ferroptosis: mechanisms, biology and role in disease. Nat. Rev. Mol. Cell Biol. 2021; 22: 266–282.

Jimsheleishvili S. & Dididze M. Neuroanatomy, Cerebellum. StatPearls, StatPearls Publishing, Treasure Island (FL). 2024.

Jovanovic M. et al. Osteogenesis Imperfecta: Mechanisms and Signaling Pathways Connecting Classical and Rare OI Types. Endocr. Rev. 2021; 43: 61–90.

Jung S.J. et al. Novel Cerebello-Amygdala Connections Provide Missing Link Between Cerebellum and Limbic System. Front. Syst. Neurosci. 2022; 16: 879634.

Juraški R.G. et al. Neurologic manifestations and sleep issues in osteogenesis imperfecta. Paediatria Croatica. 2017; 61 (3): 113-121

Kandel E.R., Schwartz JH, Jessell TM, Siegelbaum SA, Hudspeth AJ. Principles of Neural Science, Sixth Edition. Sixth Edition. Sarah Mack. 2021.

Kaur C. et al. The Choroid Plexus in Healthy and Diseased Brain. J. Neuropathol. Exp. Neurol. 2016; 75: 198–213.

Khandanpour N. et al. Craniospinal Abnormalities and Neurologic Complications of Osteogenesis Imperfecta: Imaging Overview. RadioGraphics. 2012; 32(7): 2101-12.

Kim Y.S. et al. Insights into the Dichotomous Regulation of SOD2 in Cancer. Antioxidants. 2017; 6: 86.

Klein A.P. et al. Nonmotor Functions of the Cerebellum: An Introduction. AJNR Am. J. Neuroradiol. 2016; 37: 1005–1009.

Komuro Y., Fahrion J.K., Foote K.D., Fenner K.B., Kumada T., Ohno N. & Komuro H. 2013. Granule Cell Migration and Differentiation. In: Handbook of the Cerebellum and Cerebellar Disorders (Manto M., Schmahmann J.D., Rossi F., Gruol D.L., & Koibuchi N.). Dordrecht: Springer Netherlands, p. 107–125.

Kozloff K.M. et al. Brittle IV Mouse Model for Osteogenesis Imperfecta IV Demonstrates Postpubertal Adaptations to Improve Whole Bone Strength. J. Bone Miner. Res. 2024; 19: 614–622.

Kriebel M. et al. Interference With Complex IV as a Model of Age-Related Decline in Synaptic Connectivity. Front. Mol. Neurosci. 2020; 13: 43.

Lara-Aparicio S.Y. et al. Latest research on the anatomy and physiology of the cerebellum. Neurol. Perspect. 2022; 2: 34–46.

Long K.R. & Huttner W.B. How the extracellular matrix shapes neural development. R. Soc. Open Biol. 2019; 9(1): 180216

Lv F. et al. An Update on Animal Models of Osteogenesis Imperfecta. Calcif. Tissue Int. 2022; 111: 345–366.

Marulanda J. et al. Cranio-Cervical Abnormalities in Moderate to Severe Osteogenesis Imperfecta – Genotypic and Phenotypic Determinants. Orthod. Craniofac. Res. 2024; 27: 237–243.

Marinina K.S. et al. Cognitive Decline and Mood Alterations in the Mouse Model of Spinocerebellar Ataxia Type 2. The Cerebellum. 2024; 23: 145–161.

Martins S.G. et al. Linking Oxidative Stress and DNA Damage to Changes in the Expression of Extracellular Matrix Components. Front. Genet. 2021; 12: 673002.

Nadyrshina D. et al. Osteogenesis Imperfecta: Search for Mutations in Patients from the Republic of Bashkortostan (Russia). Genes. 2022; 13: 124.

Neo S.H. & Tang B.L. Collagen 1 signaling at the central nervous system injury site and astrogliosis. Neural Regen. Res. 2017; 12: 1600–1601.

Nicol L. et al. Widespread disturbance in extracellular matrix collagen biomarker responses to teriparatide therapy in osteogenesis imperfecta. Bone. 2021; 142: 115703.

Ou M. et al. Role and mechanism of ferroptosis in neurological diseases. Mol. Metab. 2022; 61: 101502.

Palma F.R. et al. Mitochondrial Superoxide Dismutase: What the Established, the Intriguing, and the Novel Reveal About a Key Cellular Redox Switch. Antioxid. Redox Signal. 2020; 32: 701–714.

Patel V.R. & Zee D.S. The cerebellum in eye movement control: nystagmus, coordinate frames and disconjugacy. Eye. 2015; 29: 191–195.

Pavone V. et al. Early Motor Delay: An Outstanding, Initial Sign of Osteogenesis Imperfecta Type 1. J. Orthop. Case Rep. 2017; 7: 63–66.

Pei J. et al. Research progress of glutathione peroxidase family (GPX) in redoxidation. Front. Pharmacol. 2023; 14: 1147414.

Prati J.M. et al. The cerebellum and its connections to other brain structures involved in motor and non-motor functions: A comprehensive review. Behav. Brain Res. 2024; 465: 114933.

Rahimi-Balaei M. et al. Neuronal Migration During Development of the Cerebellum. Front. Cell. Neurosci. 2018; 12: 484.

Rapoport M. et al. The patient clinical journey and socioeconomic impact of osteogenesis imperfecta: a systematic scoping review. Orphanet J. Rare Dis. 2023; 18: 34.

Reeber S.L. et al. New roles for the cerebellum in health and disease. Front. Syst. Neurosci. 2013; 7: 83.

Revuelta M. et al. Glial Factors Regulating White Matter Development and Pathologies of the Cerebellum. Neurochem. Res. 2020; 45: 643–655.

Ricard-Blum S. 2011. The collagen family. Cold Spring Harb. Perspect. Biol. 3: a004978.

Schröder H, Moser N, Huggenberger S. Neuroanatomy of the Mouse: An Introduction. Springer International Publishing. 2020.

Siegenthaler J.A. & Pleasure S.J. We've got you "covered": how the meninges control brain

development. Curr. Opin. Genet. Dev. 2011; 21: 249–255.

Sgaier S.K. et al. Morphogenetic and Cellular Movements that Shape the Mouse Cerebellum: Insights from Genetic Fate Mapping. Neuron. 2005; 45: 27–40.

Shenoy M. et al. Collagen Structure, Synthesis, and Its Applications: A Systematic Review. Cureus. 2022; 14: e24856.

Shipman M.L. & Green J.T. Cerebellum and cognition: Does the rodent cerebellum participate in cognitive functions?. Neurobiol. Learn. Mem. 2020; 170: 106996.

Sillitoe R.V., Fu Y. & Watson C. 2012. Cerebellum. In: The Mouse Nervous System (Watson C., Paxinos G., & Puelles L.). San Diego: Academic Press, p. 360–397

Sinkler C.A. et al. Tissue- and Condition-Specific Isoforms of Mammalian Cytochrome c Oxidase Subunits: From Function to Human Disease. Oxid. Med. Cell. Longev. 2017; 2017: 1534056.

Song X. & Long D. Nrf2 and Ferroptosis: A New Research Direction for Neurodegenerative Diseases. Front. Neurosci. 2020; 14: 267.

Steiner R.D. & Basel D. 1993. COL1A1/2 Osteogenesis Imperfecta. In: GeneReviews® (Adam M.P., Feldman J., Mirzaa G.M., Pagon R.A., Wallace S.E., Bean L.J., Gripp K.W., & Amemiya A.). Seattle (WA): University of Washington.

Stoodley C.J. The cerebellum and neurodevelopmental disorders. Cerebellum Lond. Engl. 2016; 15: 34–37.

Sultan F. & Glickstein M. The cerebellum: Comparative and animal studies. The Cerebellum. 2007; 6: 168.

Sur S., Guler M.O., Webber M.J., Pashuck E.T., Ito M., Stupp S.I. & Launey T. 2014. Synergistic regulation of cerebellar Purkinje neuron development by laminin epitopes and collagen on an artificial hybrid matrix construct. Biomater. Sci. 2: 903–914.

Takeuchi M. et al. Type IV Collagen Controls the Axogenesis of Cerebellar Granule Cells by Regulating Basement Membrane Integrity in Zebrafish. PLoS Genet. 2015; 11: e1005587.

Tatone C. et al. Age-dependent changes in the expression of superoxide dismutases and catalase

are associated with ultrastructural modifications in human granulosa cells. Mol. Hum. Reprod. 2006; 12: 655–660.

Verkh Z. et al. Osteogenesis imperfecta type II: microvascular changes in the CNS. Clin. Neuropathol. 1995; 14: 154–158.

Wallace J.M. et al. Nanoscale morphology of Type I collagen is altered in the Brtl mouse model of Osteogenesis Imperfecta. J. Struct. Biol. 2011; 173: 146–152.

Wareham L.K. et al. Collagen in the central nervous system: contributions to neurodegeneration and promise as a therapeutic target. Mol. Neurodegener. 2024; 19: 11.

Wakamatsu K. et al. Immunohistochemical expression of osteopontin and collagens in choroid plexus of human brains. Neuropathology. 2022; 42: 117–125.

Wauquier F. et al. Oxidative stress in bone remodelling and disease. Trends Mol. Med. 2009; 15: 468–477.

Wei C. The Role of Glutathione Peroxidase 4 in Neuronal Ferroptosis and Its Therapeutic Potential in Ischemic and Hemorrhagic Stroke. Brain Res. Bull. 2024; 217: 111065.

Wenzel S.E. et al. PEBP1 Wardens Ferroptosis by Enabling Lipoxygenase Generation of Lipid Death Signals. Cell. 2017; 171: 628-641.e26.

Yoo S.-E. et al. Gpx4 ablation in adult mice results in a lethal phenotype accompanied by neuronal loss in brain. Free Radic. Biol. Med. 2012; 52: 1820–1827.

Yu H. et al. Pathogenic mechanisms of osteogenesis imperfecta, evidence for classification. Orphanet J. Rare Dis. 2023; 18: 234.

Zaripova A.R. & Khusainova R.I. Modern classification and molecular-genetic aspects of osteogenesis imperfecta. Vavilov J. Genet. Breed. 2020; 24: 219–227.

Zuo J. et al. TNF-α-mediated upregulation of SOD-2 contributes to cell proliferation and cisplatin resistance in esophageal squamous cell carcinoma. Oncol. Rep. 2019; 42: 1497–1506.